THE UNIVERSITY OF MICHIGAN
COLLEGE OF ENGINEERING

Department of Engineering Mechanics
Meteorological Laboratories

Final Report

AN INVESTIGATION OF CONVECTIVE TRANSFER PROCESSES BASED ON SATELLITE PHOTOGRAPHS

Part I

APPLICATION OF TWO-DIMENSIONAL SPECTRAL ANALYSIS TO THE QUANTIFICATION OF SATELLITE CLOUD PHOTOGRAPHS

By
Edward S. Epstein and John A. Leese

Part II

THE NATURE OF PHYSICAL PARAMETERS AFFECTING CONVECTIVE TRANSFER PROCESSES

By
John A. Leese and Charles Young

ORA Project 05068
Contract No. CWB-10062 and CWB-10062-1
under contract with
METEOROLOGICAL SATELLITE LABORATORY
UNITED STATES WEATHER BUREAU
SUITLAND, MARYLAND

Administered through:
OFFICE OF RESEARCH ADMINISTRATION
ANN ARBOR

February 1963

TABLE OF CONTENTS

ABSTRACT

Part I

APPLICATION OF TWO-DIMENSIONAL SPECTRAL ANALYSIS TO THE QUANTIFICATION OF SATELLITE CLOUD PHOTOGRAPHS

By

Edward S. Epstein and John A. Leese

Pictures from TIROS have revealed that cumuliform clouds over the ocean quite often occur in the form of a complex pattern with lines and cells of horizontal dimensions in the range of 20 to 100 miles and with various orientations seemingly superimposed. Gross features of these patterns such as the horizontal dimensions and orientation which are predominant over particular areas should prove very useful as indicators of the prevailing meteorological conditions.

A two-dimensional extension of the familiar power spectrum analysis has been applied to the TIROS photographs. The object of the analysis is to identify and quantify the statistically preferred dimensions and orientations of the cloud patterns. Digital data are derived from the photographs by adopting a simple 5-level gray scale of cloud brightness. A Monte Carlo technique has yielded estimates of the reliability of the statistical analysis.

Results from these analyses have revealed patterns which tended to be obscured by the more dominant features in addition to cloud patterns which were obvious in the original picture. The method clearly enables one to distinguish different types of cloud patterns and offers a quantification of the pictures which should aid in the interpretation and utilization of the TIROS photographs.

Part II

THE NATURE OF PHYSICAL PARAMETERS AFFECTING CONVECTIVE TRANSFER PROCESSES

By

John A. Leese and Charles Young

Cumuliform cloud patterns in the range of 25 to 100 miles are quite common over the oceans, as shown by the TIROS photographs. The lack of conventional meteorological information over most of the oceans is a major obstacle to be considered when attempting to study these cloud patterns.

Cellular convection has been the subject of many experimental and theoretical investigations since the first controlled laboratory investigations of H. Benard in 1900 and 1901. The flux of heat from the ocean to the atmosphere, and in particular, the latent heat flux must be a significant mechanism in the formation of these cumuliform clouds. A dimensional analysis of the relationship between the total heat flux and the various elements which appear physically significant reveals at least six parameters to be considered in the determination of the latent heat flux.

The practical determination of values of such parameters as the latent heat flux necessarily involves reliance on the synoptic reports of various ships. Graphical techniques appear to be the best method available to obtain the values of the parameters since smoothing is automatic in this technique. Several examples are shown to illustrate the values obtained by this method.

PART I

APPLICATION OF TWO-DIMENSIONAL SPECTRAL ANALYSIS TO THE QUANTIFICATION OF SATELLITE CLOUD PHOTOGRAPHS

INTRODUCTION

The vast number of TIROS photographs which have accumulated since the launching of TIROS I represents a challenge to meteorologists. There is an almost unbelievable amount of information contained in these pictures, but the primarily descriptive synoptic studies carried out thus far (e.g., Leese, 1962; Sadler, 1962; Staff Members, 1962; Timchalk and Hubert, 1961), have been able to extract only minor portions of it. Two reasons for this are the difficulties of obtaining any sufficiently simple and reliable relationship between the apparent surface brightness and other characteristics of the cloud cover, and the problems of quantifying, in meaningful form, the information contained in the photographs. We have applied ourselves to this second problem: the development of an objective, quantitative procedure for extracting meaningful synoptic information from the TIROS photographs. It should be added that our intent has not been to develop a real time operational technique, but rather a data reduction procedure to meet requirements for further research.

Pictures from TIROS have revealed a degree of organization in the cloud patterns covering the range of scales from the limit of resolution of the cameras up to several thousand miles. One of the outstanding features revealed by TIROS is the organization of cumuliform clouds into patterns with horizontal dimensions mainly in the range of 20 to 100 miles. The patterns sometimes occur in lines or "streets" in which case

their horizontal dimensions and orientation are quite easy to determine. However, a more common occurrence is in the form of a "vermiculated" pattern with lines and cells of various horizontal dimensions and orientation seemingly superimposed. Such patterns have been discussed by Conover (1962), and Krueger and Fritz (1961), among others. The studies of Krueger and Fritz indicate that this particular type of cloud pattern occurs in a region which has (1) a layer of moist air about 5,000 feet deep heated at the ocean surface resulting in an adiabatic lapse rate, (2) superimposed over this layer was another of greater stability which served to inhibit the convection and (3) throughout the convective layer there appeared to be little variation in wind speed and direction above that portion influenced by surface friction.

Qualitative and quantitative differences among these "cellular" patterns are immediately apparent upon even casual inspection. The significance of these differences is much less obvious, and it would appear reasonable that quantification of the patterns would be a proper, if not a necessary first step toward understanding them. The apparent quasi-periodic nature of the cloud patterns has suggested to us that two-dimensional power spectrum analysis is an appropriate technique for deriving useful numerical information from the cloud pictures.

Spectrum Analysis in Two Dimensions

While spectrum analysis in one dimension has had considerable application in meteorology, we are unaware of any previous extension of the technique to two dimensions in this context. We have recently become aware of a study by Cote, et al (1960) in which two-dimensional spectrum analysis was applied to the study of the structure of ocean waves based on stereoscopic

observations of wave heights. The analogy between their study and ours is considerable. We are concerned with atmospheric waves based on observations of the vertical motion and/or displacement of the air as evidenced by the "cellular" clouds.

Although our computing techniques were developed independently of Cote, et al, there are no substantial differences. Both are based on the methods for one-dimensional analysis described by Blackman and Tukey (1958).

In the one-dimensional time series, the autocovariance function at lag τ is defined by

$$C(\tau) = \lim_{T\to\infty} \frac{1}{T} \int_{-T/2}^{T/2} x(t) \cdot x(t+\tau)\, dt$$

where $\bar{x} = o$. This can be expressed as a Fourier transform

$$C(\tau) = \int_{-\infty}^{\infty} P(f) \exp\ [i*2\pi f\tau]\, df$$

where $i* = \sqrt{-1}$ and

$$P(f) = \lim_{T\to\infty} \frac{1}{T} \left| \int_{-T/2}^{T/2} x(t) \exp\ [-i*2\pi ft]\, dt \right|^2$$

describes the power spectrum of the stationary random process considered. Analogously, given a function of two variables, $F(x,y)$, with zero mean, one can define the autocovariance at lag (i,j) by

$$C(i,j) = \lim_{\substack{x\to\infty \\ y\to\infty}} \frac{1}{xy} \int_{-x/2}^{x/2} \int_{-y/2}^{y/2} F(x,y)F(x+i,y+j)\, dx\, dy$$

This can be written as

$$C(i,j) = \int_{-\infty}^{\infty} \int_{-\infty}^{\infty} S(\mu,\nu) \exp\ [2\pi i*(\mu i-\nu j)]\, d\mu\, d\nu \qquad (1)$$

where $S(\mu,\nu)$ describes the power spectrum of $F(x,y)$ over the two-dimensional frequency domain. When a finite series of data at equally spaced intervals are considered, the autocovariance can be evaluated only over a finite range, say $-M < i \leq M$, $-N < j \leq N$. Because of the symmetry of the autocovariances $[C(i,j) = C(-i,-j)]$ equation (1) may be represented as a cosine series

$$C(i,j) = \sum_{\mu=o}^{M} \sum_{\nu=-N+1}^{N} S(\mu,\nu) \cos\left[\pi\left(\frac{\mu}{M}i - \frac{\nu}{N}j\right)\right];$$

this can also be expressed in terms of its harmonic components as:

$$C(i,j) = \sum_{\mu=o}^{M} \sum_{\nu=o}^{N} \left[A(\mu,\nu) \sin\frac{\pi\mu i}{M} \sin\frac{\pi\nu j}{N} + B(\mu,\nu) \cos\frac{\pi\mu i}{M} \cos\frac{\pi\nu j}{N}\right]$$

where

$$\begin{aligned} S(\mu,\pm\nu) &= \tfrac{1}{2}\left[B(\mu,\nu) \pm A(\mu,\nu)\right], && \nu \neq o \\ &= B(\mu,o), && \nu = o \,. \end{aligned} \qquad (2)$$

To evaluate $S(\mu,\nu)$ write

$$C(i,j) = \sum_{\mu=o}^{M} \sum_{\nu=-N+1}^{N} S(\mu,\nu) \left(\cos\frac{\pi\mu i}{M} \cos\frac{\pi\nu j}{N} + \sin\frac{\pi\mu i}{M} \sin\frac{\pi\nu j}{N}\right), \qquad (3)$$

multiply both sides by $\cos\frac{\pi\mu' i}{M} \cos\frac{\pi\nu' j}{N}$, and sum over i and j :

$$\sum_{i=-M+1}^{M} \sum_{j=-N+1}^{M} C(i,j) \cos\frac{\pi\nu' i}{M} \cos\frac{\pi\nu j}{N}$$

$$= \sum_{i=-M+1}^{M} \sum_{j=-N+1}^{N} \cos\frac{\pi\mu' i}{M} \cos\frac{\pi\nu' j}{N} \sum_{\mu=o}^{M} \sum_{\nu=-N+1}^{N} \left[S(\mu,\nu)\right.$$

$$\times \left(\cos \frac{\pi\mu i}{M} \cos \frac{\pi\nu j}{N} + \sin \frac{\pi\mu i}{M} \sin \frac{\pi\nu j}{N}\right)] \ . \qquad (4)$$

The right-hand side of this equation can be written:

$$\sum_{\mu=o}^{M} \sum_{\nu=-N+1}^{N} S(\mu,\nu) \sum_{i=-M+1}^{M} \sum_{j=-N+1}^{N} \cos \frac{\pi\mu' i}{M} \cos \frac{\pi\nu' j}{N}$$

$$\times \left(\cos \frac{\pi\mu i}{M} \cos \frac{\pi\nu j}{N} + \sin \frac{\pi\mu i}{M} \sin \frac{\pi\nu j}{N}\right)$$

and because of the orthogonality of the cosine function, this reduces to

$$[S(\mu,\nu) + S(\mu,-\nu)] \sum_{i=-M+1}^{M} \sum_{j=-N+1}^{N} \cos^2 \frac{\pi\mu i}{M} \cos^2 \frac{\pi\nu j}{N}$$

$$= KMN[S(\mu,\nu) + S(\mu,-\nu)] \qquad (5)$$

where

$K = 1$ if $\mu \neq o, M$ and $\nu \neq o, \pm N$

$\quad\ 2$ if $\mu = o, M$ or if $\nu = o, \pm N$

$\quad\ 4$ if $\mu = o, M$ and $\nu = o, \pm N$.

Thus, equation (4) can be written

$$\sum_{i=-M+1}^{M} \sum_{j=-N+1}^{N} C(i,j) \cos \frac{\pi\mu i}{M} \cos \frac{\pi\nu j}{N} = KMN[S(\mu,\nu) + S(\mu,-\nu)] \ . (6)$$

In a similar manner it can be shown that multiplying both sides of equation (3) by $\sin \frac{\pi\mu' i}{M} \sin \frac{\pi\nu' j}{N}$ and summing yields:

$$\sum_{i=-M+1}^{M} \sum_{j=-N+1}^{N} C(i,j) \sin \frac{\pi\mu i}{M} \sin \frac{\pi\nu j}{N} = MN[S(\mu,\nu) - S(\mu,-\nu)] \qquad (7)$$

Addition and subtraction of equations (6) and (7) yield the spectral estimates:

$$S(\mu,\pm\nu) = \frac{1}{2KMN} \sum_{i=-M+1}^{M} \sum_{j=-N+1}^{N} C(i,j) \left(\cos \frac{\pi\mu i}{M} \cos \frac{\pi\nu j}{N} \pm \sin \frac{\pi\mu i}{M} \sin \frac{\pi\nu j}{N}\right)$$

$$= \tfrac{1}{2}[B(\mu,\nu) \pm A(\mu,\nu)], \quad \nu \neq o$$

$$= B(\mu,o), \qquad \nu = o \tag{2}$$

where

$$A(\mu,\nu) = \frac{1}{MN} \sum_{i=-M+1}^{N} \sum_{j=-N+1}^{N} C(i,j) \sin \frac{\pi\mu i}{M} \sin \frac{\pi\nu j}{N}$$

$$= \frac{2}{MN} \sum_{i=1}^{M} \sum_{j=1}^{N} [C(i,j)-C(i,-j)] \sin \frac{\pi\mu i}{M} \sin \frac{\pi\nu j}{N} \tag{8}$$

$$B(\mu,\nu) = \frac{1}{KMN} \sum_{i=-M+1}^{M} \sum_{j=-N+1}^{N} C(i,j) \cos \frac{\pi\mu i}{M} \cos \frac{\pi\nu j}{N}$$

$$= \frac{2}{KMN} \sum_{i=1}^{M} \sum_{j=1}^{N} [C(i,j)+C(i,-j)] \cos \frac{\pi\mu i}{M} \sin \frac{\pi\nu j}{N} \tag{9}$$

In this study, one is given the initial data $X(p,q)$, $1 \leq p \leq P$, $1 \leq q \leq Q$, at grid points over a rectangular array, and computes the autocovariance matrix:

$$C(i,j) = \sum_{p=1}^{P-i} \sum_{q=1}^{Q-j} X(p,q)\, X(p+i,Q+j)/(P-i)(Q-j) - \bar{X}^2 \quad \text{when} \quad j \geq o$$

$$= \sum_{p=1}^{P-i} \sum_{q=-j+1}^{Q} X(p,q)\, X(p+i,q+j)/(P-i)(Q-j) - \bar{X}^2 \quad \text{when} \quad j < o$$

for $o \leq i \leq M$, $-N < j \leq N$, where $\bar{X} = \frac{1}{PQ} \sum_{p=1}^{P} \sum_{q=1}^{Q} X(p,q)$.

This array is axially symmetric, so that it need not be calculated for negative values of i. Spectral estimates are then computed by applying equations (8), (9) and (2). These estimates are then smoothed by a binomial weighing function:

$$\begin{pmatrix} 1/16 & 1/8 & 1/16 \\ 1/8 & 1/4 & 1/8 \\ 1/16 & 1/8 & 1/16 \end{pmatrix}$$

which is simply a two-dimensional extension of the "Hanning" procedure recommended for one-dimensional spectrum analysis [Blackman and Tukey, 1958].

The final spectral estimates, $S(\mu,\nu)$, are available for integral values of the wave numbers in the region $-M \leq \mu \leq M$, $-N \leq \nu \leq N$. The wave number μ corresponds to a wavelength $\frac{2M\Delta x}{\mu}$ where Δx is the uniform spacing between data points in the appropriate direction of the original array.

In the actual computer program, described in the Appendix, several options are permitted. One of these is the forming of non-overlapping averages of the original data before computing the spectrum. This imposes a filter on the spectrum and rectification must be applied to the computed spectral estimates. The appropriate form of the rectification function, by which the computed spectrum is divided is (cf. Griffith, Panofsky and van der Hoven, 1956)

$$\left[\frac{\sin(\pi\mu/2M)}{\pi\mu/2M} \times \frac{\sin(\pi\nu/2N)}{\pi\nu/2N}\right]^2$$

Computer Time

Before proceeding to a discussion of the interpretation of the spectra, let us point out that their computation is a time-

consuming operation that can be carried out economically on only the fastest of available equipment. The portion of the computation requiring the most time is the evaluation of the autocovariances. Consider the case in which the initial data consists of a PXP array, and M lags are required in each direction. Altogether 2M(M+1) autocovariances are calculated, each requiring the sum of almost P^2 products. If the computation of each product, including the necessary bookkeeping and logical operations, and then forming the sum, requires 25 basic machine operations, then the total number of machine operations required for the generation of the autocovariance array is near $50P^2M(M+1)$. On the IBM 709 each machine operation requires on the average, about 5×10^{-5} sec (1×10^{-5} sec on the IBM 7090). Choosing, as an example, P = 60, M = 15, one finds that the time required to compute the array is about 36 min (7 min on the 7090). This is only one step, albeit the most lengthy, in the computation. The entire procedure for computing all the elements of the two-dimensional spectrum will require, in this case, perhaps 45 min (9 min). An outline of the program used in computing the power spectrum is given in the Appendix.

Interpretation

The computed spectrum provides estimates of the variance contributed by particular intervals of frequency. One can interpret the magnitude of the spectrum corresponding to a wave number pair (μ,ν) as representing the square of the amplitude of a wave whose normal is at an angle to the x- axis

$$\phi = \tan^{-1} \frac{\mu M \Delta y}{\nu N \Delta x} \qquad (12)$$

and having a wavelength

$$\lambda = 2\left[\left(\frac{\mu}{M\Delta x}\right)^2 + \left(\frac{\nu}{N\Delta y}\right)^2\right]^{-\frac{1}{2}} \qquad (13)$$

or better, as the extent to which waves of such characteristics contribute to the total variance of the original data. If $\Delta x = \Delta y = \Delta$, and $M = N$, the angle becomes $\tan^{-1}(\mu/\nu)$ and the wavelength $2M\Delta(\mu^2 + \nu^2)^{-\frac{1}{2}}$.

If a spectrum exhibits a single maximum (above an overall noise level), then we would expect the original data, or here the original TIROS picture, to exhibit parallel rows, or cloud "streets". If two maxima dominate the spectrum, we expect to find the interference pattern such as two waves will produce on a water surface; these are the simplest "cellular" clouds. In general, the spectra may be more complicated, with several important maxima, corresponding to quite involved patterns of interference. Two-dimensional spectrum analysis allows us to objectively determine the significant atmospheric "waves" which produce the patterns observed by TIROS. Hopefully, these will prove useful parameters in relation to significant synoptic variables for studying atmospheric convection and heat and moisture transport.

Statistical Reliability

Since an objective of the analysis is the identification of spectral maxima, it is important to know the probability that the computed spectrum will reveal maxima which are solely the result of statistical sampling fluctuation, and correspondingly, how large a maximum need be before it can be considered unlikely to have arisen by chance. For one-dimensional spectra, Blackman and Tukey (1958) have shown that $S/E(S)$ is distributed as χ^2_f/f, where S is the spectral estimate, $E(S)$ is the expected

value of S, and f, the degrees of freedom, is at least as large as $2(\frac{P}{M} - \frac{1}{3})$ if the spectrum has small slope. (Here P is the number of data points in the one-dimensional series; M is the number of lags.) Without attempting any theoretical evaluation, one might surmise that the orthogonality properties of two-dimensional spectra would yield similarly distributed estimates with $f = 4(\frac{P}{M} - \frac{1}{3})\ (\frac{Q}{N} - \frac{1}{3})$ where P and Q are the numbers of points in the x- and y- directions in the original rectangular grid, and M and N are the numbers of lags in the respective directions used in the computations. By choosing $P = Q$ and $M = N$, for simplicity, this is reduced to:

$$f = 4(\frac{P}{M} - \frac{1}{3})^2 \ . \tag{14}$$

If one applied the argument of Cote, et al to the details (especially the weights of the smoothing function) of the computational scheme which we employ, then the appropriate expression for the degrees of freedom is:

$$f = 1.80\ (\frac{P}{M} - \frac{1}{2})^2 \ . \tag{15}$$

It should be pointed out that the results of Blackman and Tukey are approximate; thus neither of equations (14) nor (15) can be accepted without some reservation. To resolve some of the uncertainties we have resorted to experimental - Monte Carlo - techniques. Matrices of numbers with known stochastic (spectral) properties are generated, and the computed spectra are compared with the expected spectra. Especially, the variances of the spectral estimates about their expected values are computed. These variances are given by

$$\hat{\sigma}_S^2 = \frac{1}{P} \Sigma\{S(\mu,\nu) - E[S(\mu,\nu)]\}^2 \tag{16}$$

where $S(\mu,\nu)$ is the spectral estimate at the wave number pair

(μ,ν) and P is the number of points over which the summation is carried out. In practice, not all wave number pairs are included in the summation since neighboring estimates are not independent. The procedure adopted is that of eliminating from the summation all points within one wave number of the limits of the spectral computation or within two of any other point already included in the summation. Thus, if $M = 10$, we include the eighteen presumably independent estimates at wave number pairs $(\pm 2,2)$, $(\pm 2,5)$, $(\pm 2,8)$, $(\pm 5,2)$, $(\pm 5,5)$, etc.

By choosing each of the original data points independently of all others (from either a uniform or Gaussian distribution), we assure that the spectrum will be "white", i.e., that $S_{\mu,\nu}$ is independent of μ and ν. The expected value of each spectral estimate is then identically $\sigma^2/2M^2$, where σ^2 is the variance of the distribution from which the initial data are chosen. If it is assumed that $S/E(S)$ is distributed as χ^2_f/f, then

$$\sigma_s^2 = \frac{2[E(S)]^2}{f} \tag{17}$$

and an estimate of the degrees of freedom is obtained from

$$\hat{f} = \frac{2[E(S)]^2}{\hat{\sigma}_s^2} = \frac{\sigma^4}{2\hat{\sigma}_s^2 M^4} . \tag{18}$$

Values of $\hat{\sigma}_s^2$ and $\hat{f}$ have been computed for a number of sets of values of P and M. These, and some auxiliary results are shown in Table 1. For comparison the values of f determined from equations (14) and (15) are also shown. Note that in all but three cases $\hat{f}$ is intermediate between the other two values, and in all but one case is greater than the value of f based on equation (15). (The values of $\hat{f}$ on lines 2 and 5 are

especially puzzling. No explanation can be offered at this writing.) A reasonable, conservative approach appears to be to use equation (15), even though most points fall closer to those of equation (14).

It now becomes possible to specify a procedure for identifying "significant" spectral maxima. The procedure for extracting the data from the TIROS photographs is crude. The cloud brightness is estimated by eye, at each point, on a scale of 0 to 4. It appears reasonable to anticipate that this procedure, together with instrumental problems that affect the picture and uncertainties as to what physical meaning one should attach to apparent cloud brightness, might result in a standard error of estimate, $\sigma \approx 1$. If the parameters from which the spectrum is computed are, say, $P = 50$, $M = 12$, then from equation (14) we find $f \approx 25$, and a noise level of $\frac{1}{2}(\frac{\sigma}{M})^2 = .0035$ is anticipated. The upper 1% limit of χ^2_f/f for $f = 25$ is 1.77. Then, if $S > 0.0035 \times 1.77 = 0.0062$, the peak can be considered to be real and not the result of sampling fluctuations.

Another approach to estimating the noise level is by examination of the spectrum. One normally finds that a general noise level (perhaps somewhat "red" noise, increasing toward lower frequencies) is clearly defined. In other words, most of the spectrum is relatively flat, with a few regions showing slightly less variance and others considerably more. If the level of the relatively flat portion is taken as the noise level, this corresponds quite well to that given in the previous paragraph (i.e., $\sigma \approx 1$), or is even somwhat lower.

In general, several real spectral maxima appear in the spectra of the TIROS pictures; it has not been difficult to find

Table 1. Results of Monte Carlo Experiments

Array Size N	Lags	Distribution*	Number of Spectra	Number of Points P	Spectral Estimates Expected ($\times 10^2$)	Spectral Estimates Mean ($\times 10^2$)	Degrees of Freedom $\hat{f}$	Degrees of Freedom Eq(14)	Degrees of Freedom Eq(15)
16	7	U	10	80	5.36	5.01	11.2	15.2	5.75
25	7	U	10	80	5.36	5.43	78.1	41.9	17.0
25	10	U	10	180	2.62	2.67	24.3	18.8	7.20
30	10	G	4	72	0.500	0.520	15.6	28.4	11.2
32	7	U	5	40	5.36	4.96	15.8	71.8	29.8
32	10	U	5	90	2.62	2.59	24.5	32.9	13.1
32	13	U	5	160	1.55	1.55	14.5	18.1	6.93
48	13	U	5	160	1.55	1.57	40.0	45.1	18.3
48	20	U	5	216	0.656	0.673	14.3	17.1	6.50

* G = Gaussian
U = Uniform

or isolate "real" spectral peaks. Rather, it seems necessary to consider only those maxima which contribute the most to the total variance, occasionally neglecting small but statistically significant peaks. The 1% level of significance is used throughout this paper.

IDEALIZED CLOUD PATTERNS

As a test of the spectral analysis techniques, several idealized patterns with different dimensions and orientations, were constructed. These idealized patterns were made up of a combination of the two basic patterns shown in Figure 1.

The interpretation of complicated patterns similar to those found in actual cloud pictures is illustrated by a combination of patterns 1 and 2 plus a random noise superimposed on the composite. Pattern number 1 was oriented at an angle of 135 degrees to the x-axis and pattern number 2 was oriented at an angle of 30 degrees. Equally spaced data in a rectangular array were derived from this composite by, effectively, an averaging procedure; each element, or square, was assigned a value from 0 to 4. The input points for this pattern are shown in Figure 2. The important features of the spectrum of this pattern are known; spectral peaks should occur as given in Table 2. They are numbered in descending order of magnitude. The dominant wave should be the one oriented at 30 degrees with a wave-length of 5 units.

Table 2. Values of parameters, μ, ν, ϕ, and λ with composite pattern made up of No. 1 at 135 degrees and No. at 30 degrees.

MAX No.	1	2	3	4
μ	2.4	2.4	0.6	1.2
ν	4	-2.4	-1.5	1.2
ϕ	30	135	120	45
λ	5	7.07	8	14.14

In order to more realistically duplicate an actual cloud pattern a Gaussian noise was superimposed on this composite pattern. This noise was in the form of a set of random numbers with a mean of 0 and a standard deviation of 1.5.

When the noise was added the data points were allowed to range only from 0 to 7 . All negative numbers were given the value of 0 and any number greater than 7 was assigned the value of 7 . Thus the actual noise was artificially skewed, and had a somewhat smaller standard deviation.

The final pattern in the form of a square array with 36 data points in each direction is shown in Figure 3. An analysis of this square array was performed using a maximum lag of 12 in each direction. The autocovariance coefficients obtained from this pattern are shown in Figure 4. Harmonic analysis and smoothing produces the spectrum illustrated in Figure 5. The large amount of noise superimposed on this pattern, together with the size of the array and the number of lags used, requires, according to the previous section, that the spectral maxima be greater than 1.7×10^{-2} to be considered significant. The parameters relevant to the three significant peaks shown in Figure 5 are given in Table 3.

Table 3. Values of parameters, μ, ν, ϕ, and λ actually obtained from spectral analysis of composite pattern.

MAX No.	1	2	3
μ	2.4	2.7	1
ν	4	-2.2	1
ϕ	30	129	45
λ	5	7.02	16.8

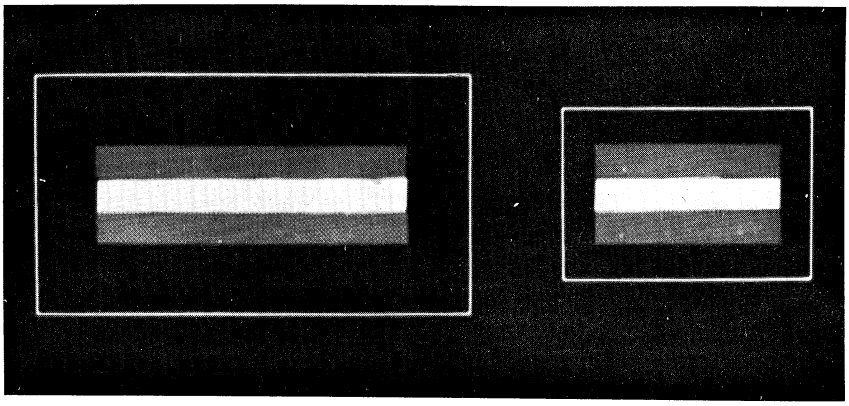

Figure 1. Basic patterns used as input data to construct idealized cloud pattern. (Pattern number 1 on left; number 2 on right)

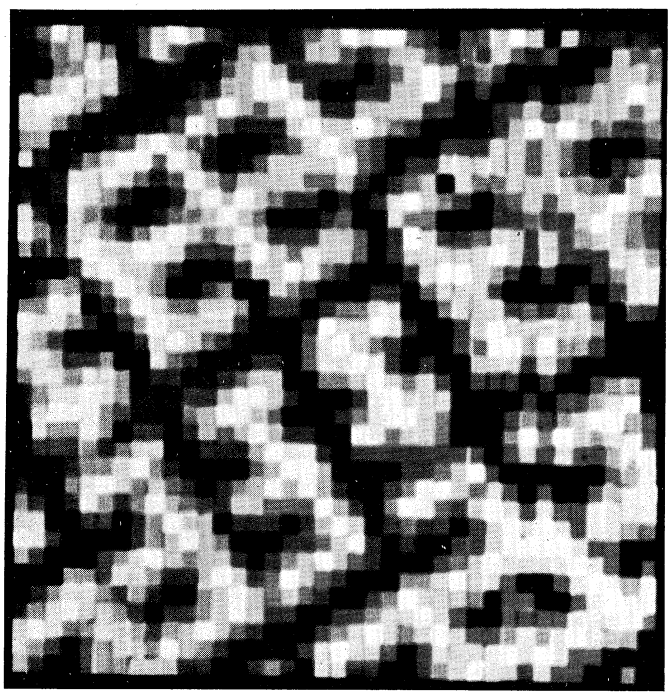

Figure 2. Input data for pattern number 1 oriented at an angle of 135 degrees and pattern number 2 at an angle of 30 degrees.

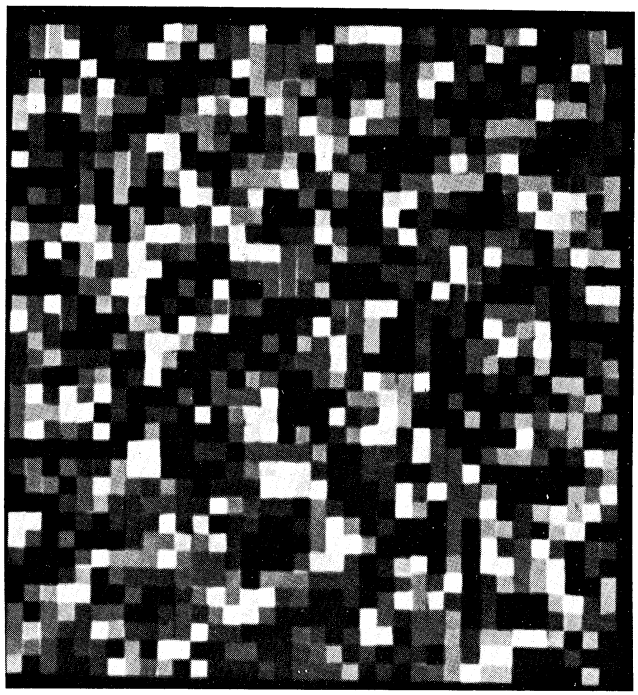

Figure 3. Input array of Figure 2 with a random noise superimposed.

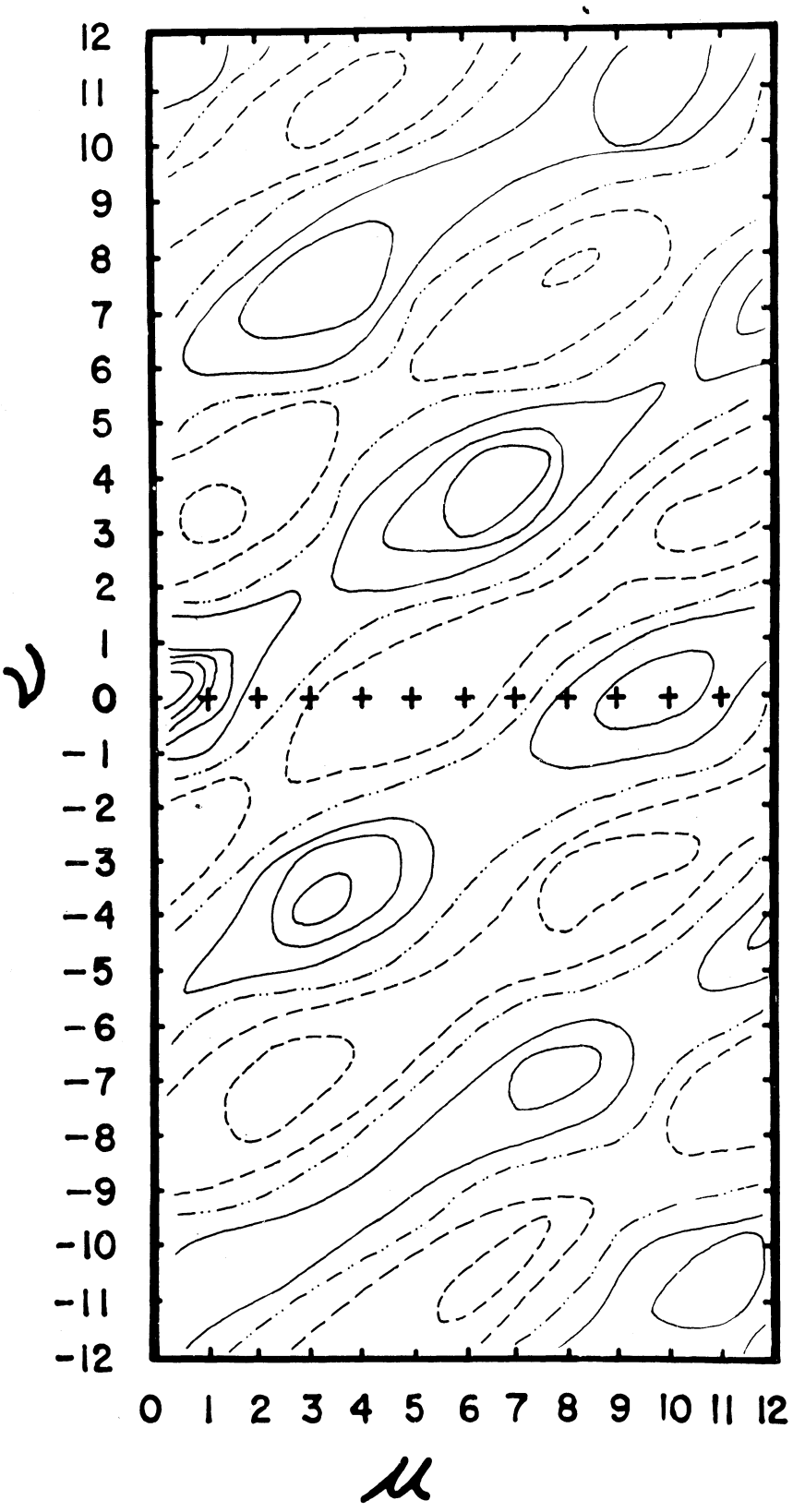

Figure 4. Autocovariance pattern obtained from analysis of array shown in Figure 3. (Solid lines: positive; dashed lines: negative; contour values: 0.2, 0.5, 0.8, 1.0, 2.0, etc.)

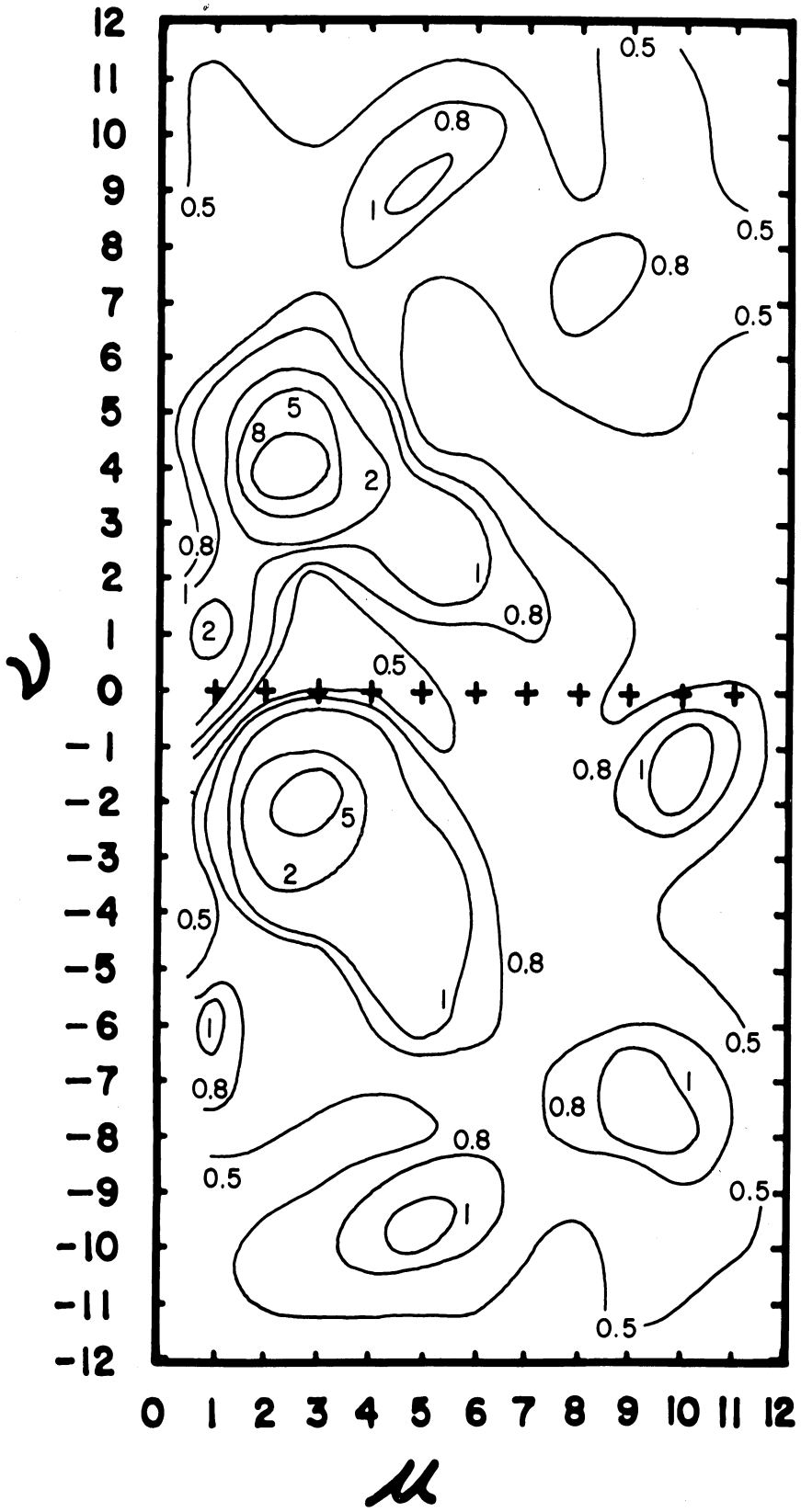

Figure 5. Spectral pattern for array shown in Figure 4. (All values multiplied by 100.)

A comparison of these results with those expected from the input pattern, Table 2, shows that the dominant pattern with an orientation of 30 degrees and a wavelength of 5 units agrees exactly. The second and third expected spectral peaks are not resolved, but are combined into a single maximum in the computed spectrum. The result of combining these two maxima yields a wave with an orientation of 129 degrees and a wavelength of approximately 7 units. The results obtained from this and other idealized patterns (not shown) demonstrate the ability of this two-dimensional spectral analysis technique to separate periodic phenomena from a substantial amount of noise. They also illustrate the limitations of the technique due to the low resolution at the lower frequencies. Greater resolution can be achieved only by using larger numbers of lags, but this has a corresponding deleterious effect on the degrees of freedom and the reliability of the spectral estimates.

ANALYSIS OF TIROS PICTURES

Data

Pictures transmitted from TIROS were available on strips of 35 mm film. In order to utilize this type of analysis with the TIROS pictures, it was necessary to convert to digital data evaluated at equally spaced intervals. Digital data were derived from the pictures by adopting a simple five-level gray scale of cloud brightness ranging from zero for clear through four for the brightest clouds in the picture. Since TIROS is oriented in space the usable nadir angle can vary from zero to 65 degrees (horizon for altitude of TIROS). In order to achieve equally spaced data it was necessary to take out the perspective caused by changes in the angle of view on a spherical earth.

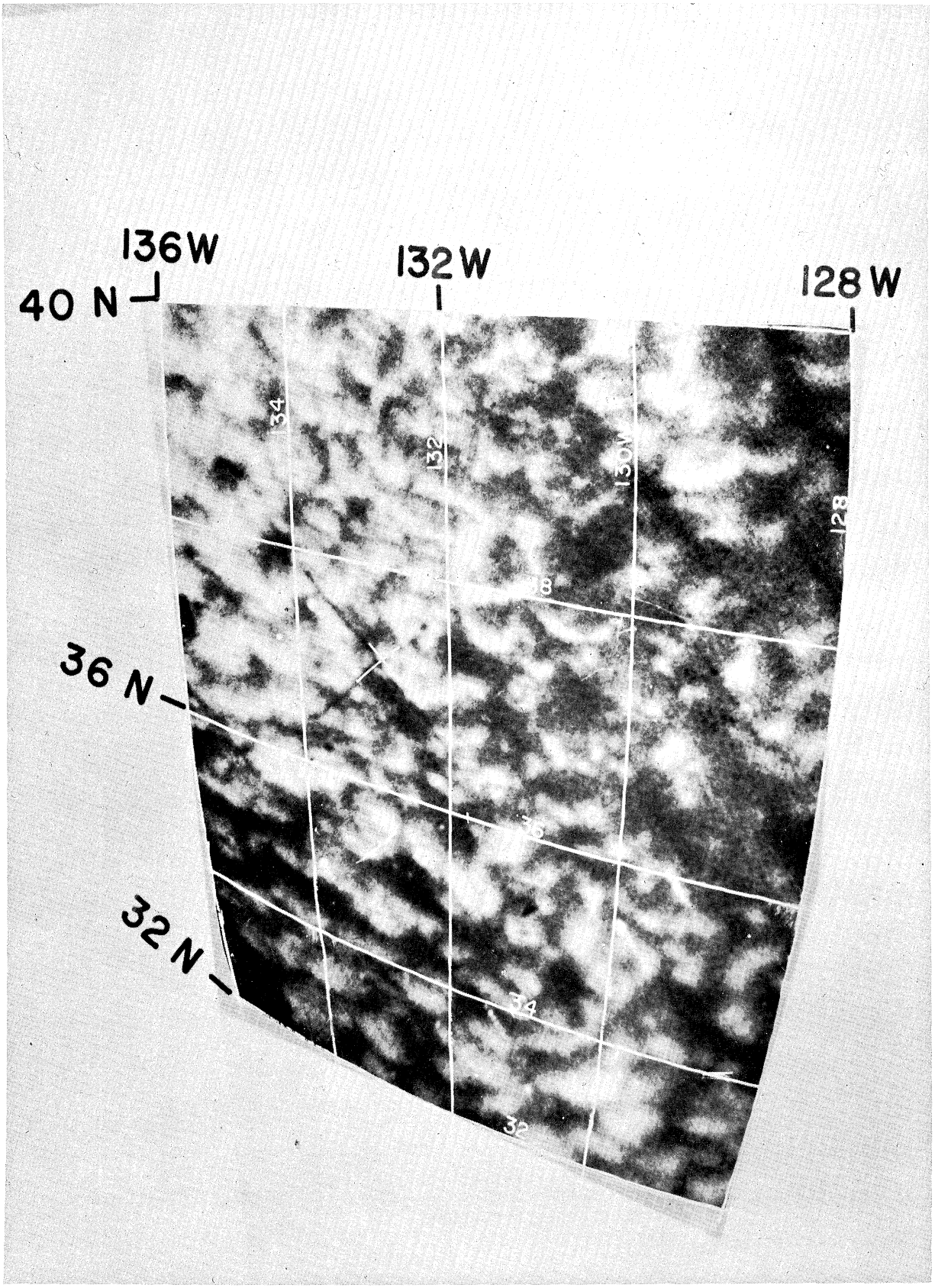

Figure 6. "Vermiculated" pattern, Eastern Pacific, 2130 GMT, May 21, 1960.

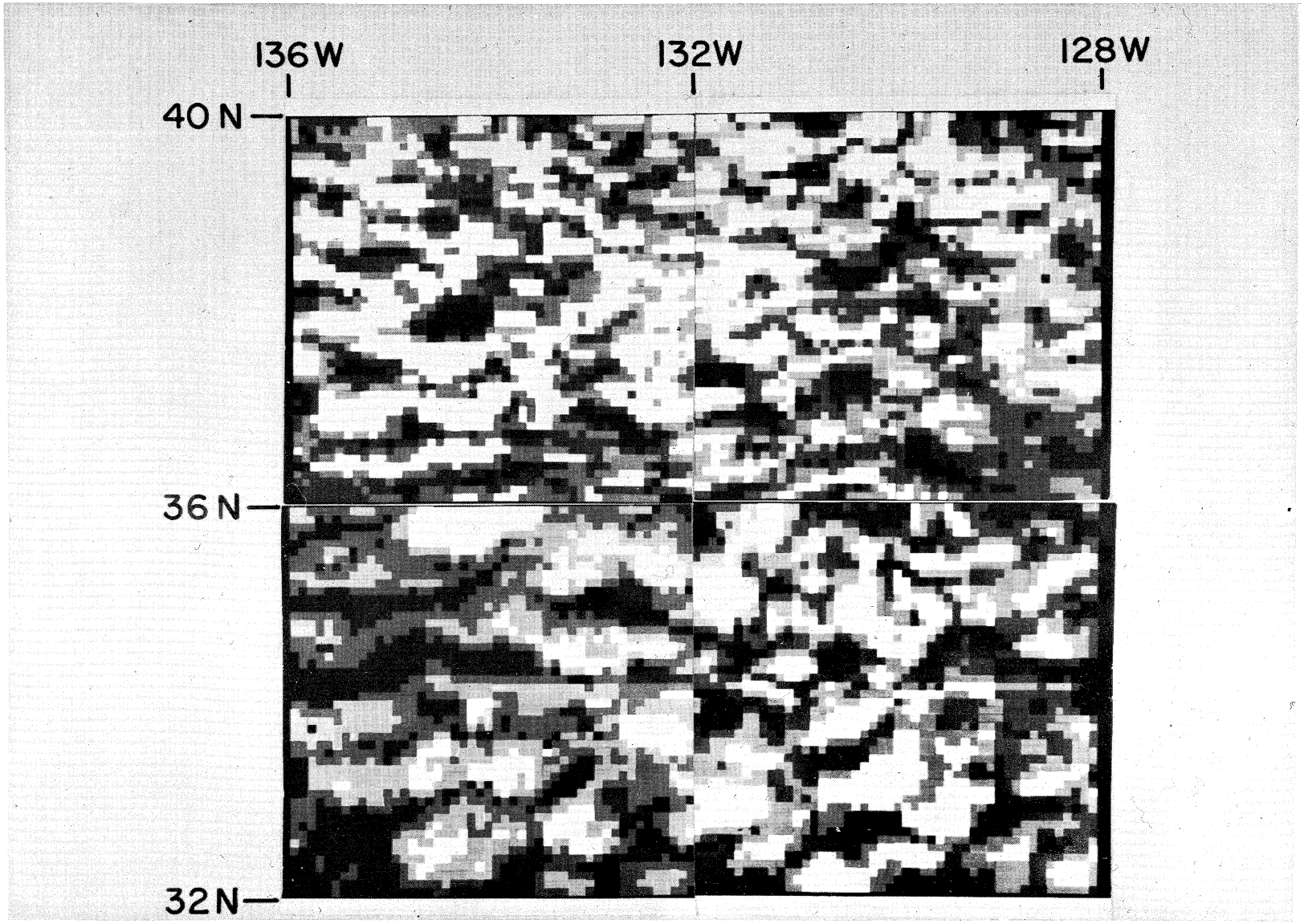

Figure 7. Reproduction of Figure 6 using equally spaced digital data.

In the initial stage, enlarged photographs with grids of latitude and longitude superimposed for every two degrees were provided by the Meteorological Satellite Laboratory of the U.S. Weather Bureau. It was assumed that variation in size due to perspective was linear within any two degree square. By restricting the pictures used to nadir angles of 50 degrees or less and utilizing the data near the principal point of the picture, it is felt that errors introduced by this assumption have been kept to a minimum. Each two degree square to be used was then subdivided into smaller squares five miles on a side. The gray scale value for each 5 mile square was then read off by eye.

It is not possible to evaluate the amount of error which may have been introduced by using this rather crude method of extracting the data, particularly when this is considered in comparison to the uncertainties of the relationship of apparent brightness to sun angle, cloud thickness, water content, etc. To provide some idea of our ability to simulate the actual cloud pattern, one of the pictures was converted back to a black and white image from the digital data using craftone paper. The original picture is shown in Figure 6. The image reproduced from the digital data is shown in Figure 7. The striking similarity of the reproduction to the original picture allowed us to conclude that this method of digitalizing the picture is adequate for our purpose.

For pictures in which latitude and longitude grids were not available, the positive film strips were used directly. This method has the advantage of using transmitted light from a variable source as opposed to reflected light from a photographic image. The pictures were rectified to take out the

perspective, but no attempt was made to utilize an axis of latitude and longitude since it is quite easy to transform our axis to that of latitude and longitude when the need arises.

Since the type of cloud pattern of interest to us is quite common over the oceans, TIROS satellites have provided innumerable photographs which could be analyzed. The choice of specific cases to be analyzed was dictated mainly by the availability of conventional meteorological observations in the region for later correlation between the results of the spectral and synoptic analyses.

Orbit 732, Frame 10, May 21, 1960

Pictures taken by TIROS I at approximately 2130 GMT on May 21, 1960, showed an extensive area of the "vermiculated" pattern off the West Coast of the United States. Frame 10 of this sequence of pictures showed this area best in terms of complete coverage and acceptable nadir angle. A grid of latitude and longitude was superimposed on this picture by the Meteorological Satellite Laboratory of the U.S. Weather Bureau. Cloud densities were assigned to each five mile square covering the area shown in Figure 6. An area approximately 480 miles on a side was coded into a two-dimensional array of 96 x 96 data points.

The results of a spectral analysis of this array using a maximum lag of 24 in each direction are shown in Figure 8. The spectral energy is concentrated in the region of low wave number pairs with the major peak located at (0,0). Other than the peak located at the origin there is only one other which can be resolved. The location of this peak of spectral energy is at $\mu = 2$, $\nu = 4$. Substituting these values in equations (12) and (13) yields a wave oriented at 27 degrees with a wavelength of approximately 55 miles. The significance of this

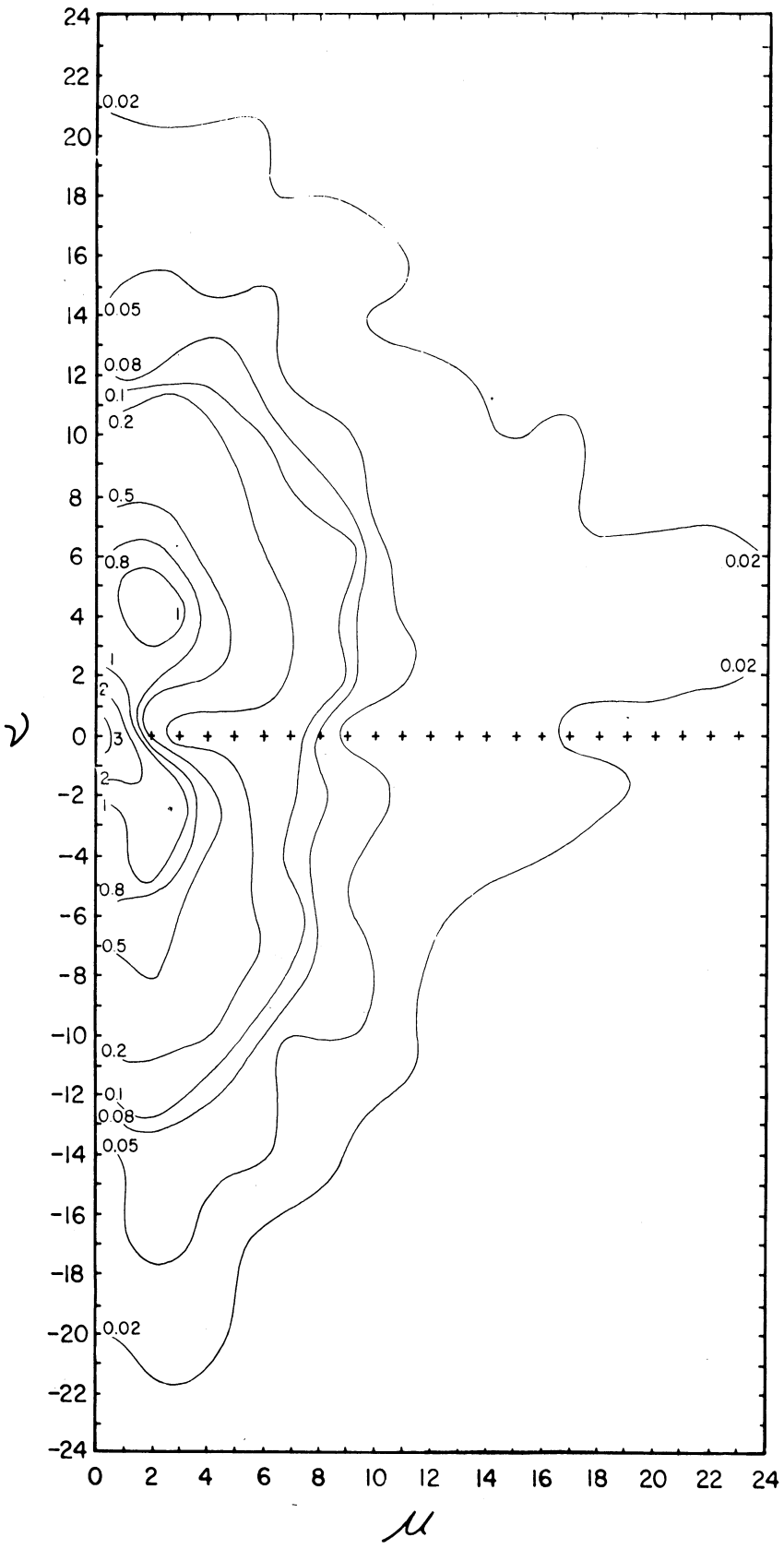

Figure 8. Spectral pattern obtained from analysis of cloud pattern shown in Figure 7. (All values multiplied by 100.)

result, however, is questionable, since it is apparent from the original picture that this spectral peak results from a heterogeneous combination of a number of patterns with different dimensions and orientations, each characteristic of smaller sections of the 480 mile-square region.

The concentration of variance near the wave pair (0,0), and then falling off rapidly, is primarily the result of gradual changes of mean cloudiness across the areas studied. This could be a real change or a spurious one caused by sun "glint" on the clouds. It would be advantageous to eliminate effects such as sun "glint". Since large scale variations in cloudiness did not seem pertinent to our objective of describing the "cellular" patterns, we have adopted a pre-whitening procedure which eliminates this effect. A further reason for eliminating this effect is that the analysis of statistical reliability by Blackman and Tukey, as well as our own Monte Carlo experiments, presuppose that the true spectrum varies slowly with frequency. The pre-whitening procedure eliminates the resulting large spectral slope near the origin which was detrimental in terms of our ability to specify the reliability of the results.

Pre-whitening was accomplished, prior to computing the autocovariance, by fitting a plane ($x_c = a + bi + cj$) by least squares to the initial data. The spectral analysis is then carried out for the residual $x'(i,j) = x(i,j) - x_c(i,j)$. This eliminates almost all variance at (0,0) and has negligible effect away from the origin, leaving the more pertinent portions of the spectrum undisturbed.

An obvious conclusion to be drawn from Figure 8 is that it was necessary to increase the resolution in the range where the spectral energy was concentrated. This can be accomplished either by increasing the number of lags or by increasing the data

interval (i.e., by decreasing N/M, but holding $N\Delta x$ constant). The latter course was chosen primarily for the economic reasons of minimizing computing time. The data interval was effectively doubled by using 2 x 2 non-overlapping averages, and subsequently dividing by the appropriate filter function. Further computations of the spectral pattern utilizing the same input data and the modifications outlined above did in fact yield considerable improvement in our ability to resolve the spectral peaks. However, they also yielded fairly convincing proof that an input pattern such as this, in which it is possible to pick out as many as six different patterns by eye in the original picture, produced spectral patterns which were complicated beyond our present ability to interpret them properly.

Although the area covered by this array is made up of cloud patterns with large variations in dimensions and orientation, a closer examination reveals that these variations appear to be segregated into separate sections with each having a predominant set of dimensions and orientation. This suggests that a great deal more quantitative information could be derived from this picture by computing power spectra for individual sections of the picture. This also aids in the interpretation of the spectral analysis pattern for the whole area. Thus the grid of 96 x 96 data points was subdivided into four sections. A 2 x 2 averaging was used and spectral patterns were computed for each of these sections using a maximum lag of 12 in each direction. The arithmetic mean was also computed for the four sections. These values of N and M were chosen in an effort to maximize the resolution at relatively low frequencies, recognizing the cost in terms of fewer degrees of freedom, i.e., four for each quadrant's spectrum. It was necessary to have spectral estimates (S) greater than 1.15×10^{-2} to be considered significant.

The boundaries of the four regions are shown in Figure 9. Reference can be made to Figure 6 for details of the actual cloud pattern in each of these regions.

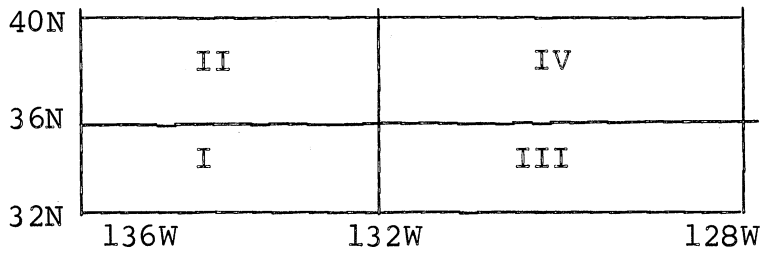

Figure 9. Boundaries of the four regions of Figure 6 for which separate spectral patterns were computed.

Region I was composed of long lines approximately parallel to the East-West axis. The primary spectral peak (Figure 10) occurs at $\mu = 1$, $\nu = 5$. The maximum at this wave number pair corresponds to a wave oriented at 11 degrees to the East-West axis with a wavelength of 48 miles. This result is in excellent agreement with the original picture which contained five distinct lines of cloud within its 240-miles width. A wave which lies exactly parallel to the x-axis would produce a spectral peak which occurs along both the positive and negative axes of the spectrum. Since this pattern was not exactly parallel to the axis there is only a partial reflection in the spectral energy for $\nu < 0$ in the vicinity of $\mu = 1$, $\nu = -5$. The peak of spectral energy poorly resolved at approximately $\mu = 0.8$, $\nu = 1.2$ is apparently related to the lateral width and orientation of brighter areas along the long lines of clouds. This wave, with an orientation of 146 degrees and a wavelength of 167 miles, would interfere with the primary wave to produce lines of elongated cloud cells. However, very little confidence can be placed in the dimensions and orientation determined by using a wave number less than one.

Region II contained a larger percentage of cloud cover than did Region I. Although some lines were evident in the cloud pattern, the overall view was that of a polygonal-shaped pattern. The spectral analysis of this region (Figure 11) showed two distinct maxima. The first peak was at the wave number pair (2.2, 3.8) and the second at (2.8, -2.1). The first maximum yields a wave oriented at 30 degrees with a wavelength of approximately 54 miles. The second corresponds to a wave oriented at 127 degrees with a wavelength of approximately 68 miles. Cloud patterns with dimensions and orientations close to those shown by the spectral analysis can be found in the original cloud pattern. These superimposed waves and their interference pattern give the overall impression of a polygonal-shaped pattern. The two maxima located at $\nu = 7$, and -7 with $\mu < 1$ are at too low a frequency for quantitative interpretation, but suggestions of corresponding patterns can be discerned, a posteriori, in the picture.

An examination of the clouds making up Region III does not reveal much in the way of an organized pattern. The spectral analysis pattern of this region (Figure 12) shows four maxima. The location of these maxima as well as the resultant orientation and dimensions of the patterns are given in Table 4.

Table 4. Location of maxima and resultant patterns from a spectral analysis of Region III.

MAX No.	1	2	3	4
μ	2.3	2.5	3	1.4
ν	2.5	5.0	2	-4.7
λ	137	27	56	163
ϕ	70	42	67	49

The first maximum is the result of a change in cloud brightness due to a regularity in a noise pattern over an interval of television scan lines. This cannot be considered as a real change in the cloud pattern. Cloud patterns with the dimensions and orientations of those given by the other three maxima can be found in this region, although no clearly predominant pattern can be detected visually. According to the spectral analysis the wave oriented at 27 degrees with a wavelength of 42 miles is of slightly more significance than the others.

The regularity of the noise occurring over an interval of television scan lines also complicated the spectral analysis pattern of Region IV. Of the three maxima shown in Figure 13 only one can be ascribed to the actual cloud pattern, and this has only marginal significance. The peak in the spectral energy located at $\mu = 2.8$, $\nu = 9.9$ is the result of a cloud pattern oriented at 16 degrees with a wavelength of 24 miles. The other two maxima located at wave number pairs of (1.4, -1.5) and (3.2, -3.5) yield waves with each oriented at 137 degrees and wavelengths of 117 and 51 miles respectively. This orientation is that of the television scan lines to the East-West axis. The wavelengths are the dimensions of the interval over which the noise occurred regularly while the picture was being received.

The spectral analysis pattern resulting from the whole area can now be examined with a knowledge of the contributions made by the various cloud patterns. The peak of spectral energy located at the wave number pair (2,4) (Figure 8), is primarily the result of the cloud patterns from Regions I and II. Cloud patterns can be found in the picture which contributed to the large area of high values in the spectral energy around wave number pair (2, -2). However, the major contribution has been

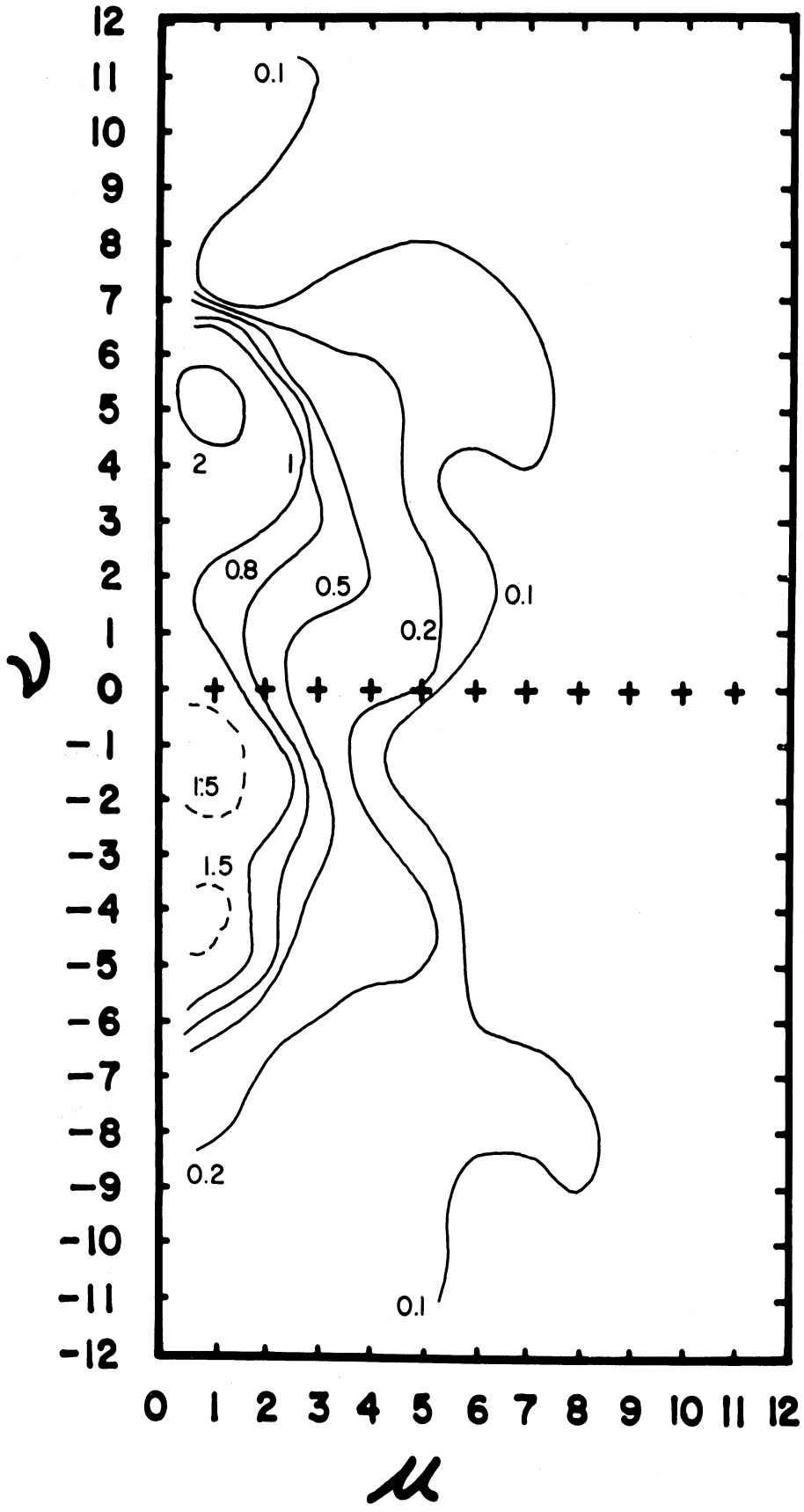

Figure 10. Same as Figure 8 for Region I.

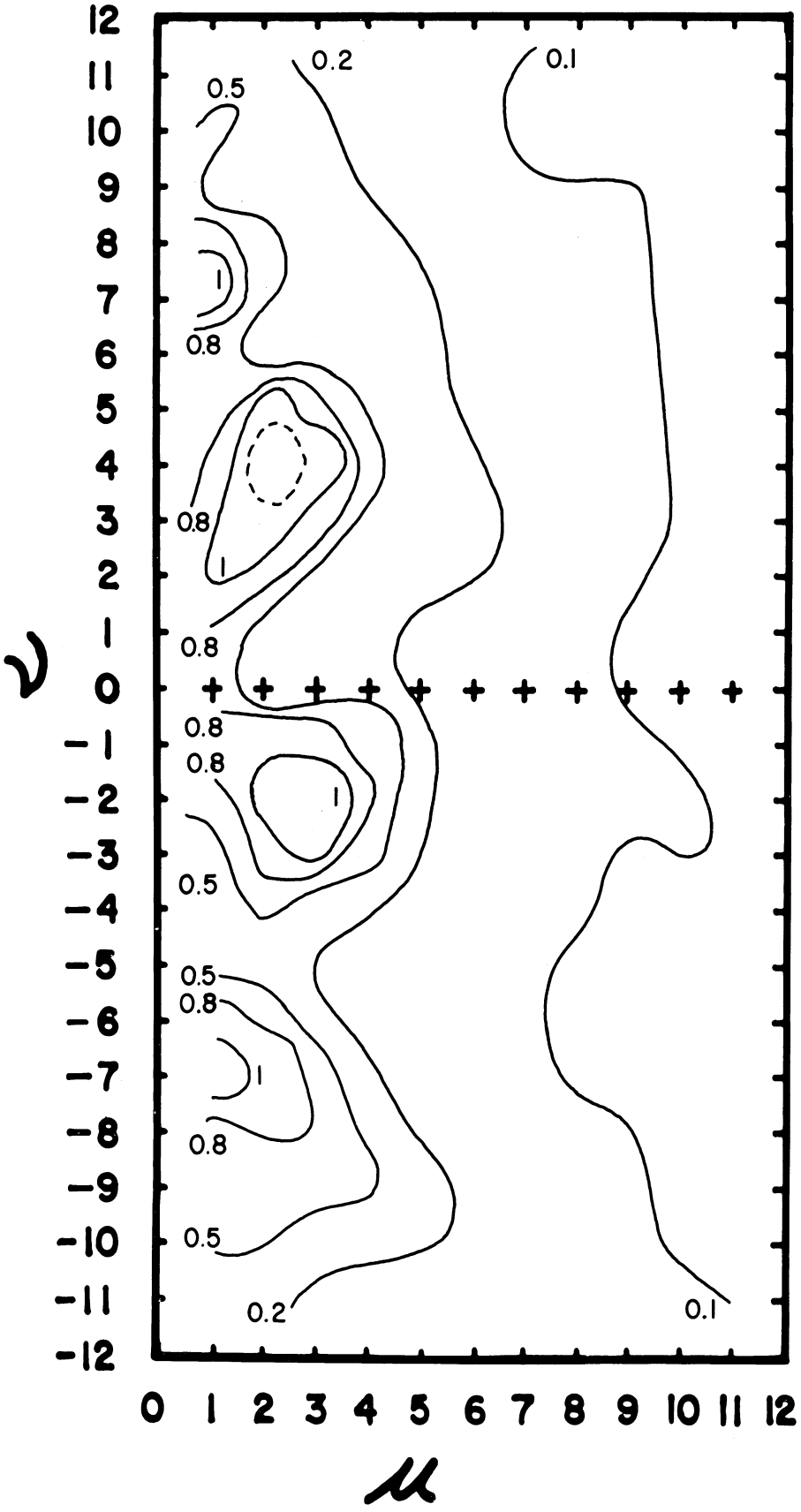

Figure 11. Same as Figure 8 for Region II.

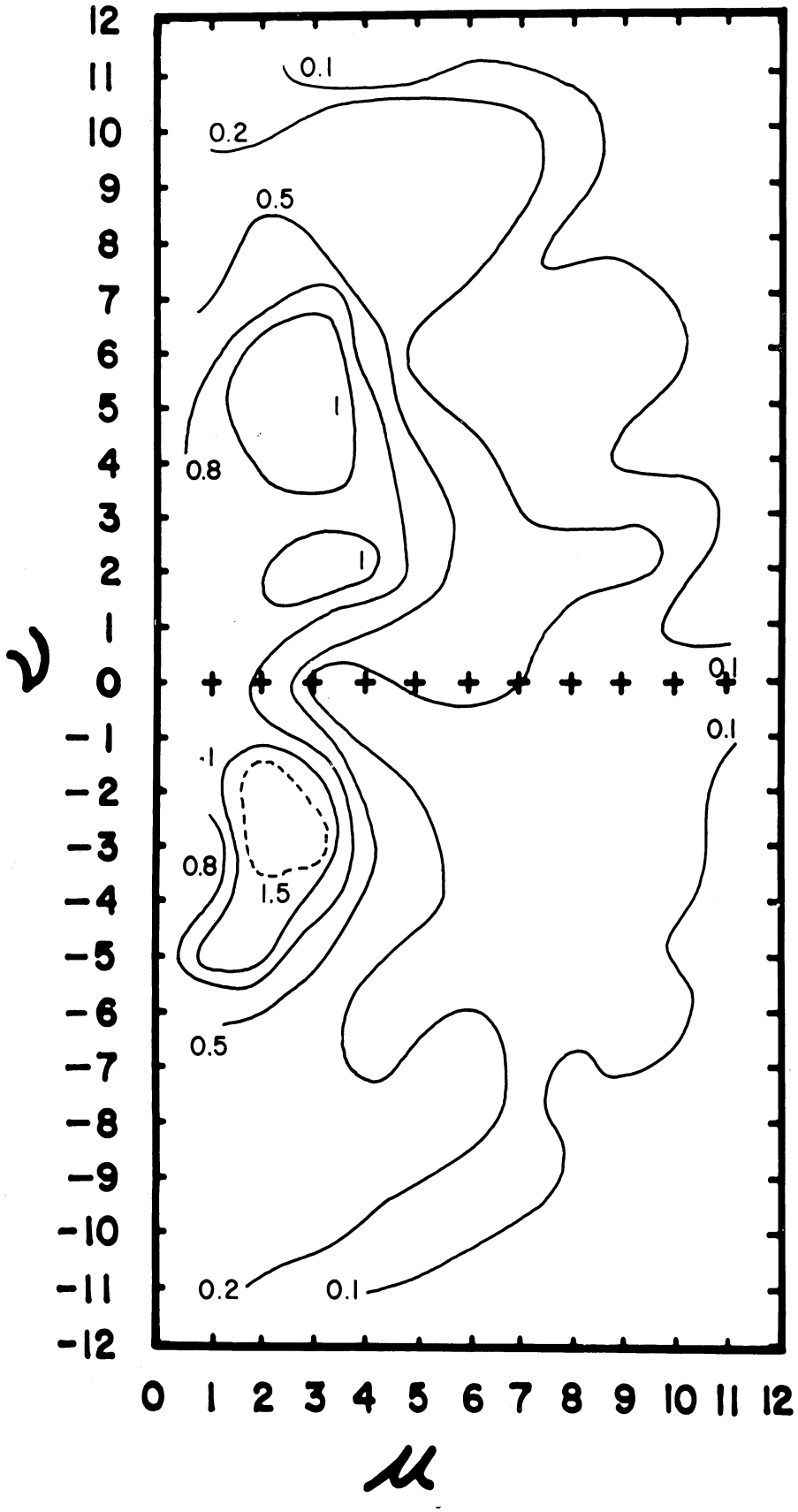

Figure 12. Same as Figure 8 for Region III.

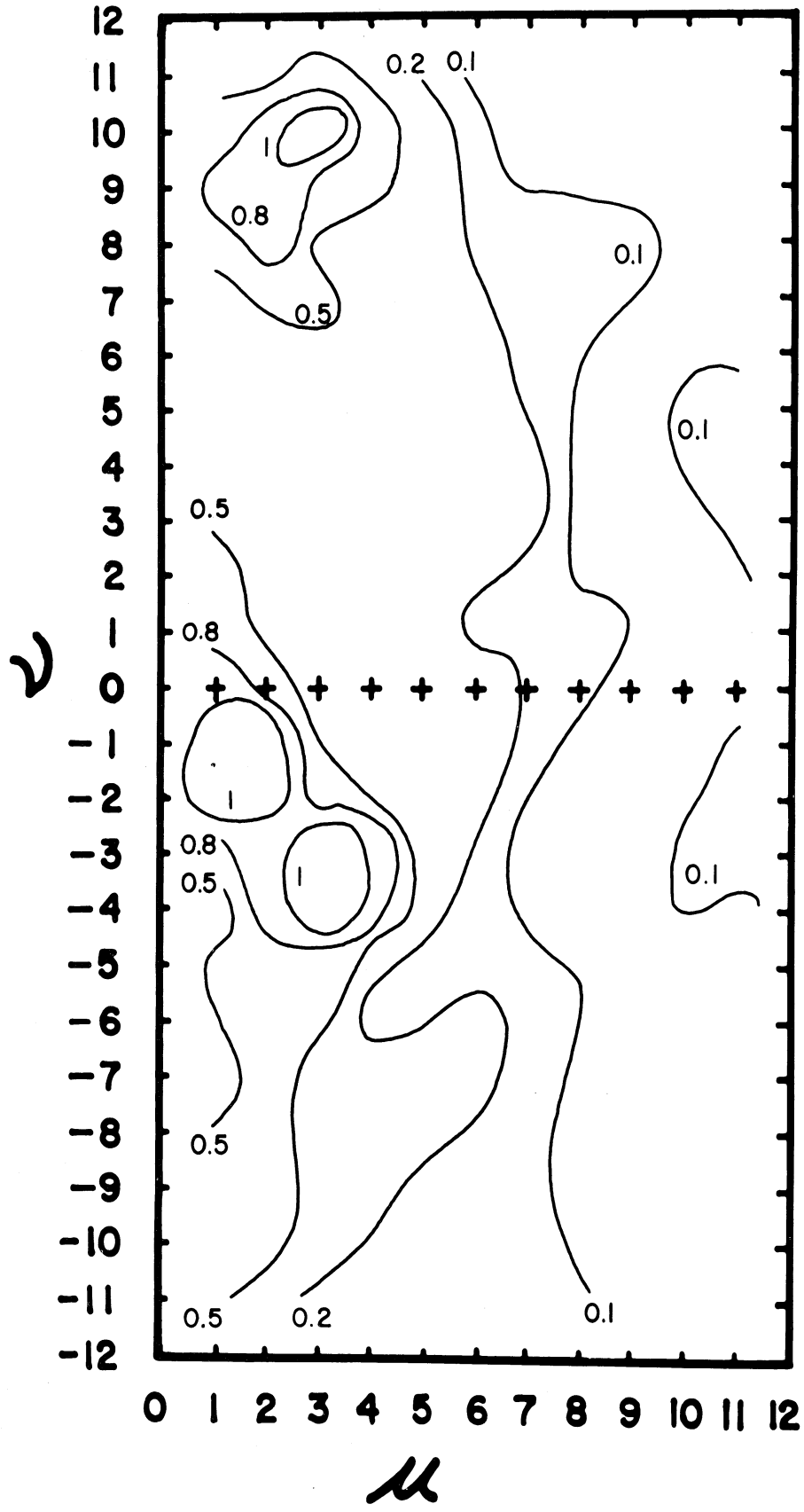

Figure 13. Same as Figure 8 for Region IV.

the result of the regular noise patterns over an interval of television scan lines in Regions III and IV.

Orbit 104, Frame 28, April 8, 1960

A very extensive area covered by "vermiculated" clouds was found on a picture taken at approximately 1430 Z on April 8, 1960 (Figure 14a). A square region of 600 miles on a side was mapped on this picture using x and y coordinates as defined by the perspective grid. The location of this area is shown in Figure 14b. This large area was subdivided into four equal sections and transformed into two-dimensional arrays with 60 x 60 data points. The boundaries of these four sections are shown in Figure 14c.

The spectral patterns (not shown) for each section using a maximum lag of 20 in each direction revealed that nearly all the energy was concentrated in the lower wave number pairs. A relatively small but significant peak of energy occurred in each of regions V and VI at the approximate wave number pair (13,3). These peaks are the result of a wave oriented at 75 degrees with a wavelength of approximately 14 miles. An examination of the original picture showed that these peaks of energy were both the result of a regular noise pattern in the television scan lines. In an effort to achieve greater resolution at the lower wave numbers, the data interval was effectively doubled by using a 2 x 2 averaging. Spectral patterns were computed for each of the four sections, plus an arithmetic mean, using a maximum lag of 12 in each direction. With these parameters it was necessary to have a spectral estimate (S) greater than 0.89×10^{-2} in order to be considered significant.

The cloud pattern in Region V presents the appearance of being very complex. The results of a spectral analysis of this

Figure 14a. Cumuliform cloud pattern, Central Atlantic, 1430Z, April 8, 1960.

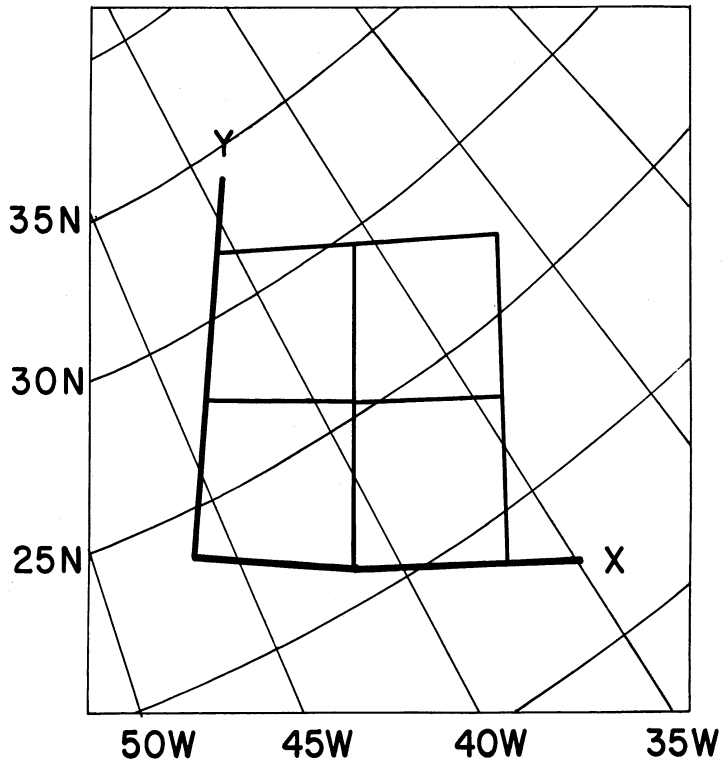

Figure 14b. Geographical location of Figure 14a.

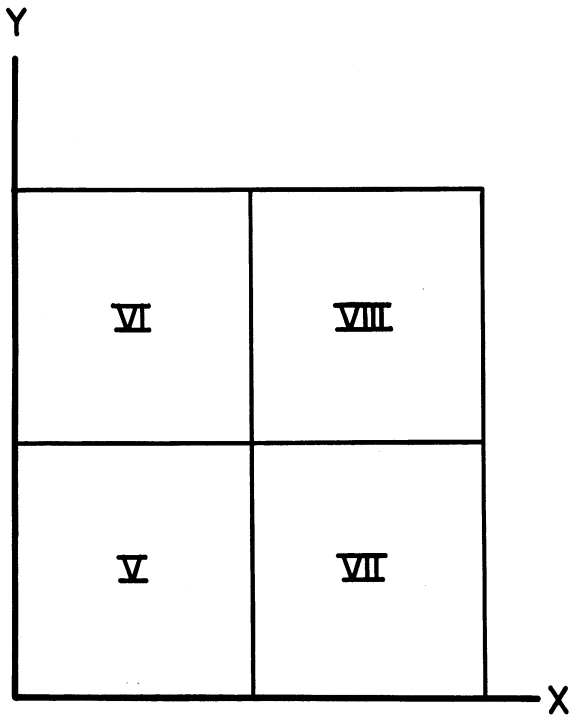

Figure 14c. Boundaries of the four regions of Figure 14a for which separate spectral patterns were computed.

cloud pattern, shown in Figure 15, seem to confirm this fact in that there are three distinct maxima present. However, when the original cloud pattern and spectral pattern are examined together it is found that the cloud pattern is much less complex than it appears, and also that a fourth maximum is present in the spectral pattern. The dominant peak in the spectral pattern, located at the wave number pair (1.1, 3.3), delineates the predominant cloud pattern within the region. The peak of energy at this wave number pair is the result of a wave oriented at 18 degrees to the x-axis with a wavelength of 69 miles. This wave is not immediately obvious in the original picture but can be found in the form of five distinct lines of clouds oriented at a small angle to the x-axis. The original cloud picture contains evidence that the relatively flat region around this peak is the result of an unresolved maximum near the wave number pair (2,4). This unresolved peak is associated with the peak in the negative quadrant located at (2,-4). These two peaks are the result of waves approximately 54 miles in length with the former oriented at 27 degrees and the latter at 153 degrees to the x-axis. They are the result of cloud lines which are bent approximately like gull's wings, in the original picture. The maximum located at the wave number pair (8,-5) has a maximum spectral estimate of 0.94×10^{-2} which is only slightly above the value of 0.89×10^{-2} which is needed in order to be considered significant. Cloud patterns oriented at 122 degrees with a wavelength of approximately 25 miles which contributed to this peak are not obvious in the original picture.

The pattern (Figure 16) which resulted from a spectral analysis of the clouds in Region VI presents one of the simplest cases to interpret. Although the maximum value of the spectral energy occurred in the neighborhood of the wave number pair

(0,0), this can be attributed to contributions from several sources to be discussed later. The two significant peaks associated with the cloud patterns are those located at (8.2, -2.3) and (7, -4). The former pair is the predominant in terms of magnitude of the spectral energy and is also obvious in the original cloud picture. The cloud pattern oriented at 106 degrees to the x-axis with a wavelength of approximately 28 miles is found in the upper half of Region VI (Figure 14a). The peak located at (7, -4) is the result of a cloud pattern oriented at 120 degrees with a wavelength of approximately 30 miles. A pattern having these dimensions and orientation is present in the lower half of Region VI of the original cloud picture.

The fact that this type of analysis will invariably attempt to resolve the lateral dimensions of waves present in the pattern has been pointed out many times already in the report. The spectral pattern of this region demonstrates how this factor may be used as an aid in avoiding misinterpretation of the location and sizes of the spectral peaks. The relatively flat peak in the neighborhood of the wave number pair (0,0) can be attributed to three major contributions of this type. As a first approximation the wave made up by the lateral width will be perpendicular to the original wave. An inspection of the cloud pattern in the original picture will yield a qualitative estimate of the dimensions of the lateral width. A knowledge of these two facts can then be used to estimate the region of the spectral pattern in which the maximum should appear. In this manner it is possible to determine that the maximum in the spectral pattern near the wave number pair (0,0) is the result of the lateral dimensions of the wave associated with the peak at (8.2, -2.3).

It can be shown in a similar manner that the ridge of relatively large, though not statistically significant, spectral estimates near (3,2) may be associated with the lateral dimensions of the wave with peak energy at (7, -4). In the analysis of this region, prior to performing the 2 x 2 averaging, it was found that a regular noise pattern in the television scan lines resulted in a relatively small but significant peak in the spectral pattern. Although this wave has largely been filtered out, the lateral dimensions are still present, and it is this factor which contributed to the relatively large values in the spectral pattern near (1, -3).

The spectral analysis of some of the previous pictures have served to call attention to cloud patterns which were not obvious in the original picture. That this type of analysis can also show the opposite effect can be seen by comparing the spectral patterns obtained from an analysis of regions VII (Figure 17) and VIII (Figure 18) with the original cloud pictures. The spectral patterns show relatively large amounts of energy throughout the low wave numbers. However, neither of these patterns showed any clearly defined peaks with the wave number $\mu > 1$. The maximum located at the wave number pair (1, 3.3) in Figure 17 is the result of a wave oriented at 17 degrees with a wavelength of approximately 70 miles. A cloud pattern with the dimension and orientation similar to this wave is not obvious in the original cloud picture. Cloud patterns can be found in these two regions with dimensions of approximately 30 miles. However, the orientation of these particular cloud patterns throughout the region is so scattered that a dominant pattern cannot be resolved with the number of lags and data interval used. Thus, what appears to be a dominant pattern by visual inspection of

the cloud picture is found to be essentially a random pattern due to the various orientations which exist in this range of dimensions.

In an effort to improve the resolution in the y-direction, the data from Regions VII and VIII were combined to form a rectangular array of 60 x 120 data points. Non-overlapping averages were computed using two data points in the x-direction and three in the y-direction. The maximum number of lags used was 12 and 15 for the x and y-directions, respectively. With the size of the array and the number of lags used, a spectral estimate with a magnitude greater than 0.65×10^{-2} was required, in order to be statistically significant.

The spectral pattern for the combined regions (Figure 19) shows a maximum at the wave number pair (1,5.5). The resultant wave with a length of approximately 77 miles and an orientation of the wave resulting from the spectral peak at (1, 3.3) in Figure 17. The fact that this pattern can be resolved in the spectral analysis of the combined regions and still not be apparent in the original cloud picture emphasizes the potential value of the spectral analysis. A relatively small but statistically significant peak at (1.3, 8.9) has been resolved in the analysis of the combined regions, but was not present in the spectral patterns of the individual regions (Figures 16 and 17). Since the dimensions in the x-direction have not been changed, the peak would have occurred at the wave number pair (1.3, 4.7) in the spectral patterns of the individual regions. Although no maximum occurred, the spectral estimates were high enough to be statistically significant at this point in both regions. This would indicate that the maximum at (1.3, 8.9) in Figure 19 is the result of the increased resolution rather than an increase

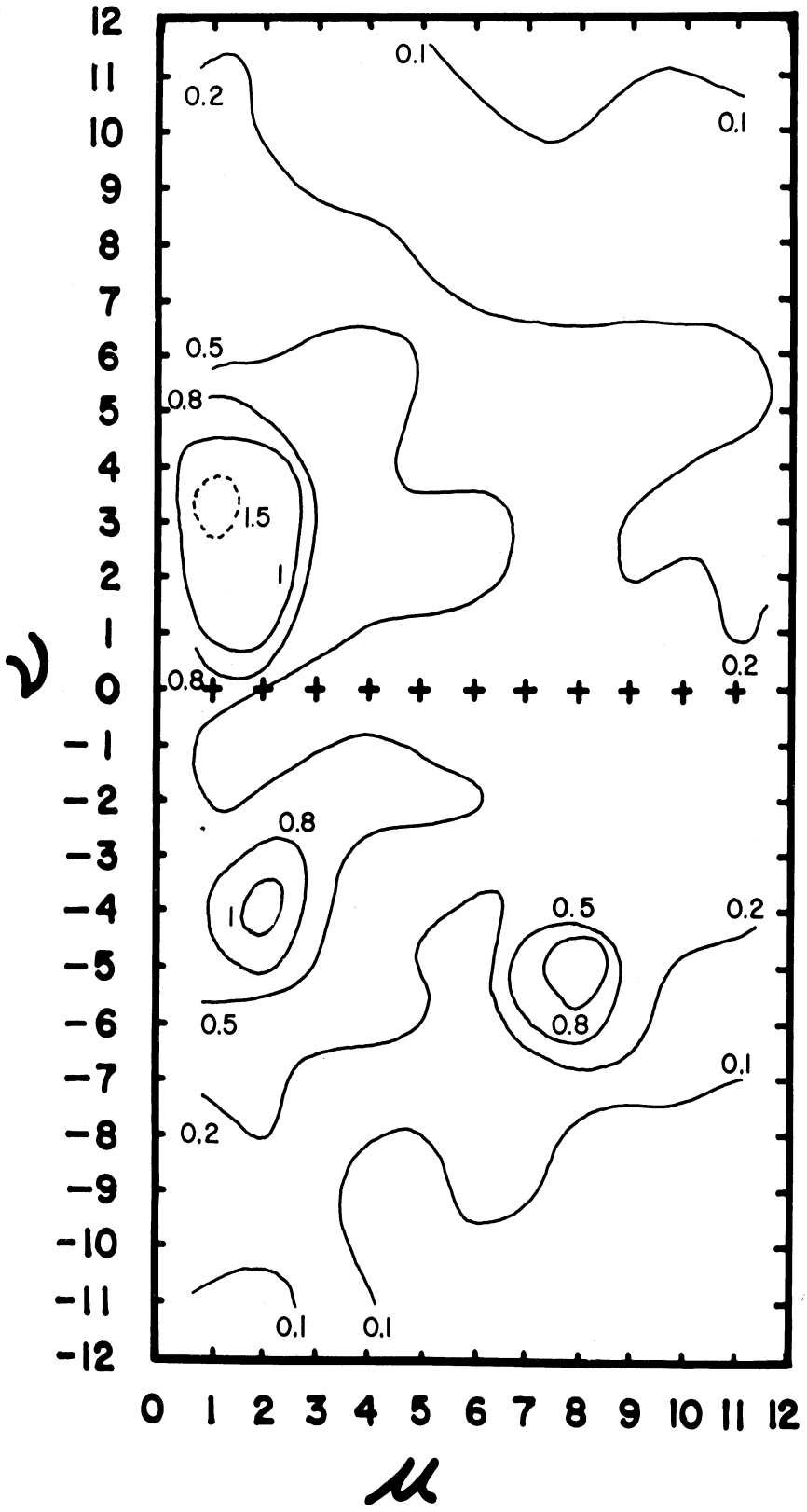

Figure 15. Spectral pattern obtained from analysis of cloud patterns of Region V shown in Figure 14. (All values multiplied by 100.)

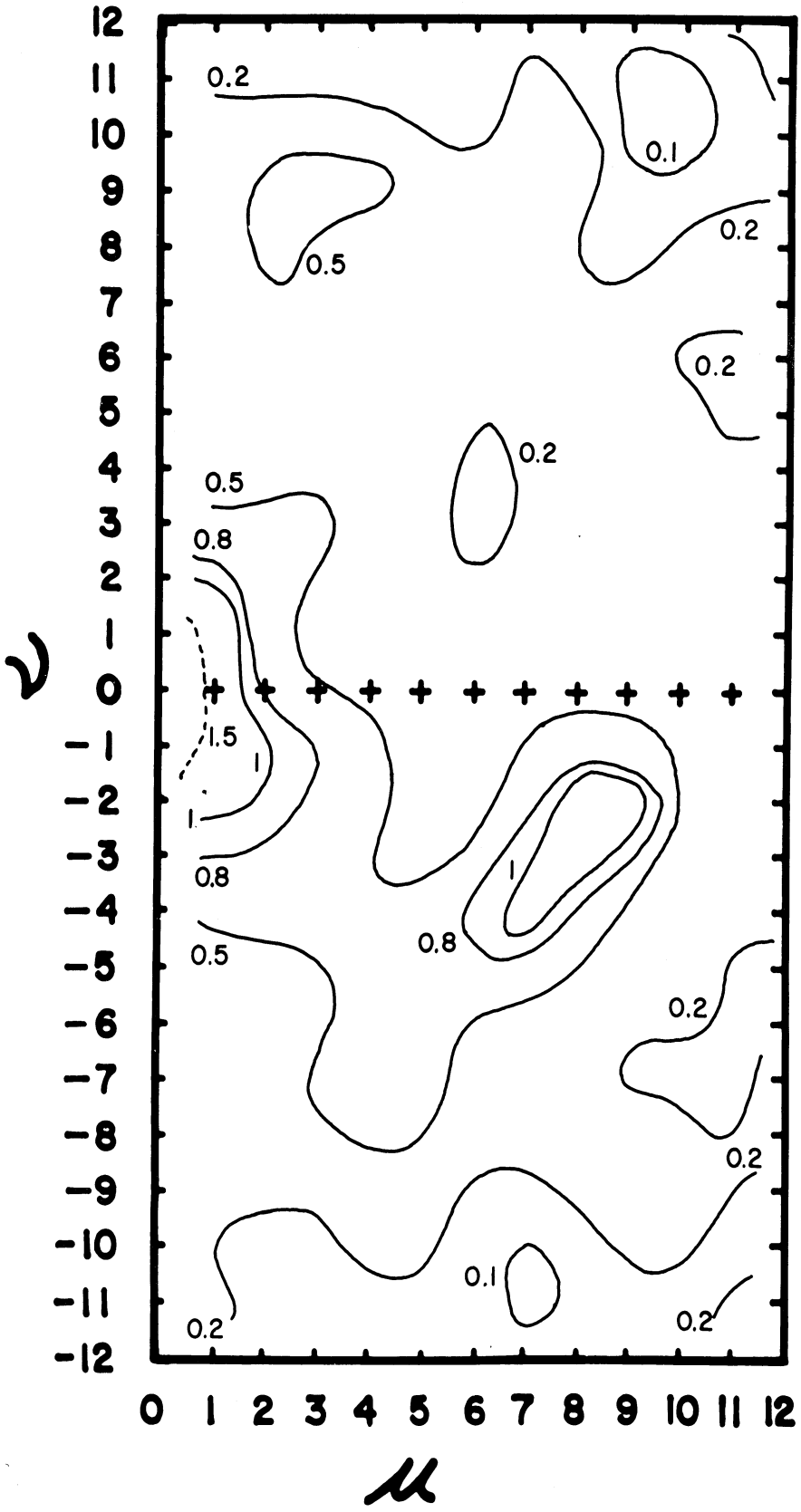

Figure 16. Same as Figure 15 for Region VI.

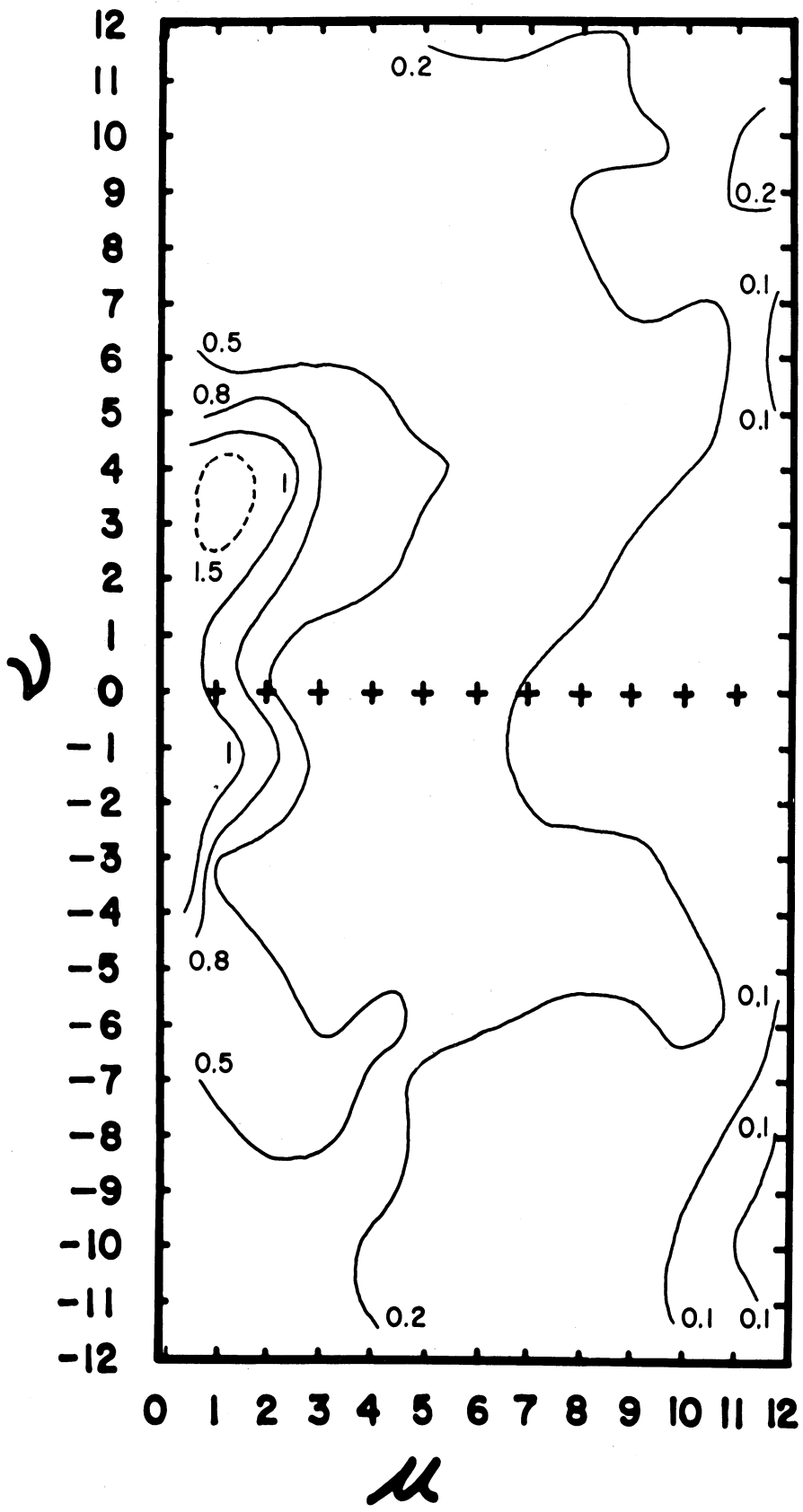

Figure 17. Same as Figure 15 for Region VII.

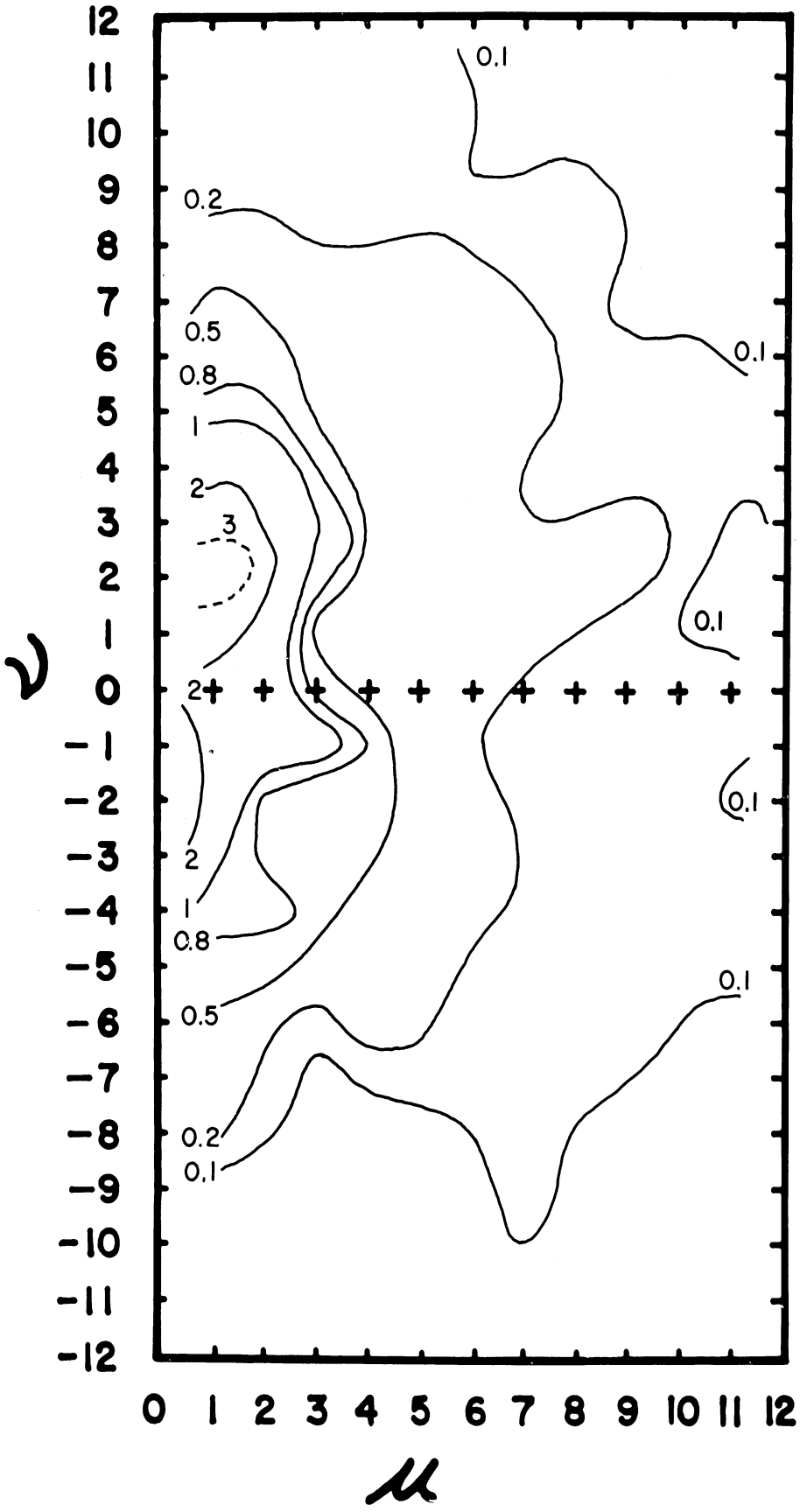

Figure 18. Same as Figure 15 for Region VIII.

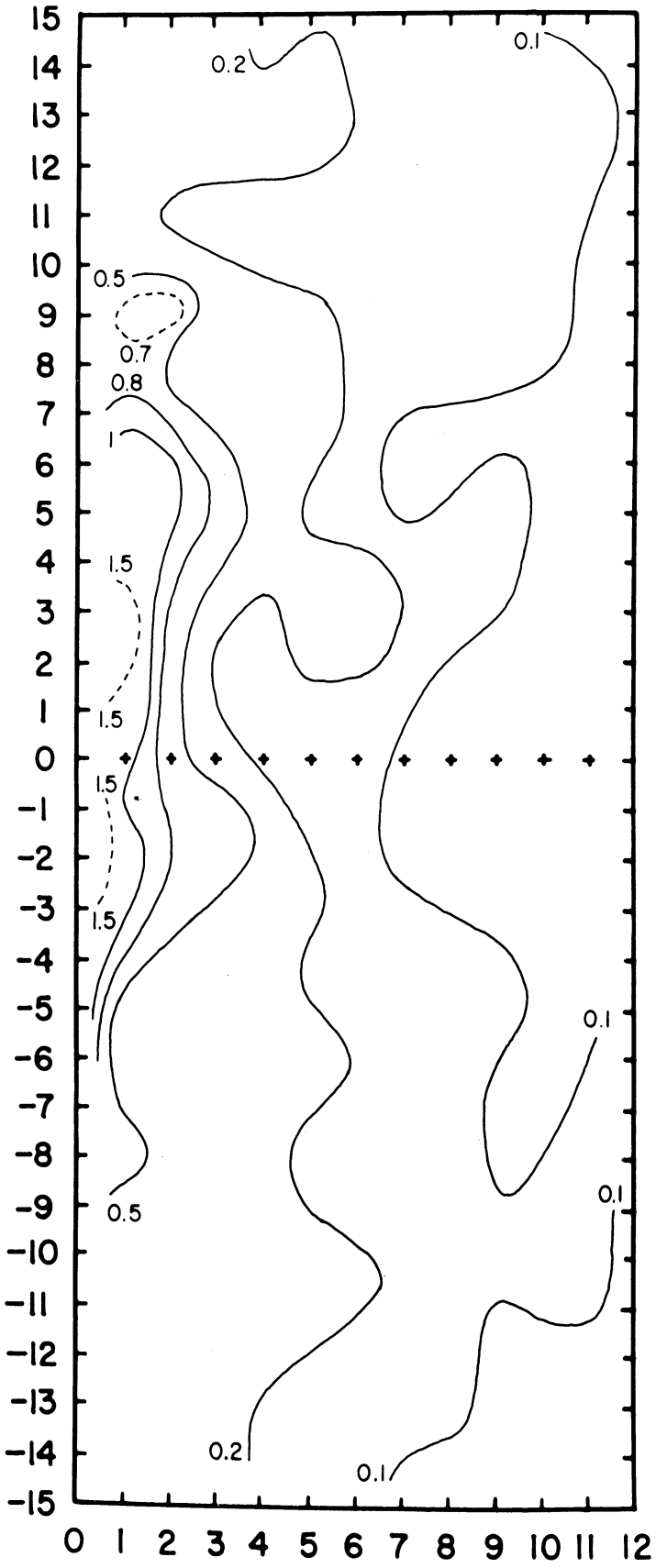

Figure 19. Same as Figure 15 for Regions VII and VIII combined.

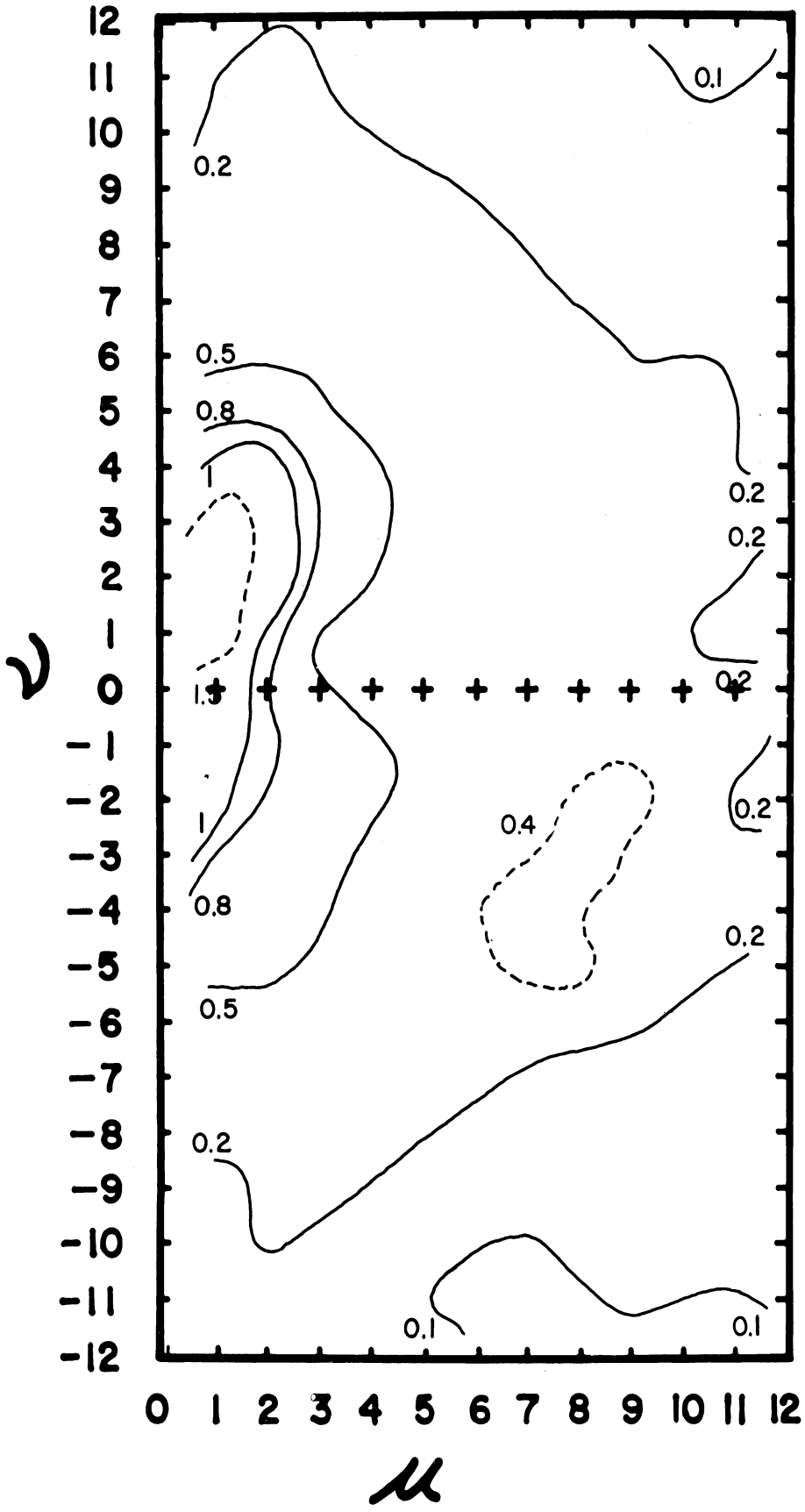

Figure 20. The mean spectral pattern for Regions V - VIII.

in the spectral estimate obtained by combining the two regions. It seems plausible to expect that peaks similar to this could be resolved in the x-direction if the resolution was not restricted by the size of the array.

The spectral patterns for the four regions can now be combined to form an average for the whole area. This may be considered as an average made up of four independent samples so that the degrees of freedom are also increased. This serves to decrease the limiting value of spectral estimates for statistical significance to 0.6×10^{-2}. The mean of the spectral patterns from the four regions shown in Figure 20 exhibits characteristics similar to those found in the spectral pattern (Figure 8) which resulted from an analysis of Figure 6. The one significant peak occurring in Figure 20, located at the wave number pair (1,2), like the one in Figure 8, is the result of a combination of many patterns and cannot be attributed to any single pattern in the original picture. It is of interest to note that the cloud patterns which dominated Region VI do not achieve statistical significance in the spectral pattern. The maximum value within this area is only 0.47 versus the value of 0.60 required for significance at the 1% level. Thus, it is not possible to specify a predominant cloud pattern for the combined regions with the resolution available in Figure 20.

OTHER METHODS OF ANALYSIS

An increase in the size of the area used in this type of analysis not only makes it possible to achieve better resolution, but is actually a requirement. The dimensions of the cloud patterns require a large number of lags in order to achieve the required resolution with the data interval of five miles. Accuracy of the spectral estimates imposes restrictions on the

maximum number of lags which can be used. However, the amount of computational work required imposes a more severe restriction on the number of lags which can be used. Thus, the only alternative available is to increase the size of the data interval. The averaging technique used in this study proved to be a most effective means to increase the data interval.

The data interval was effectively increased by using $m \times n$ non-overlapping averages, and subsequently dividing by the appropriate filter function. With one exception, the cases described in this study have used $m = n = 2$. When Regions VII and VIII were combined, to form a 60×120 array, the averages were computed using $m = 2$ and $n = 3$. In an effort to optimize the determination of the spectral patterns, i.e. maximum resolution and minimum computing time, several regions were recomputed using $n = m = 3$. In order to maintain reasonable stability of the spectral estimates, it was also necessary to reduce the number of lags used. The net effect of this was to move the peaks in the spectral pattern away from the low wave numbers, but because the number of lags used had to be decreased, the resolution was not changed significantly. It is obvious that a further increase in the data interval by the averaging technique combined with a decrease in the number of lags used would result in a decrease in resolution of the spectral pattern. Furthermore, it can be seen that an optimum method for computing the spectral pattern for any given photograph does exist, but this is determined by such factors as the dimensions of the cloud elements and the size of the area covered by a "stochastically stationary" cloud pattern.

A method which also has the effect of increasing the size of the data interval is to use only every nth point in the

original array. Several computations using $n = 2$ (result not shown) were carried out. In general the noise level by this method is greater than by that of computing averages, as the averaging over an n x n region reduces the standard error of extimate of each point (assuming independence) by $1/n$. In order to reduce the noise level of the spectra obtained from the partial grid to that obtained from the averages, it would be necessary to compute the n^2 possible individual spectra (omitting different data each time), and to average these. This, however, would defeat the objective of obtaining higher resolution at relatively low frequencies with a minimum of computing time. The non-overlapping averages produce the desired result, and since the effects of this technique on the spectral estimates are known (Griffiths, Panofsky and Van der Hoven, 1956), it was considered the better method to use in this study.

CONCLUSION

The use of two-dimensional spectral analysis techniques has been very limited up to now. Thus, it has been necessary that the first major effort in this study be devoted to refinements in the development of the technique and especially along the lines of the interpretation of the spectral patterns obtained.

The results of the analysis of the idealized cloud patterns have demonstrated the ability of this technique to separate the periodic phenomena from a substantial amount of noise and have also been useful by showing the limitations of this technique. The results of analysis of actual cloud pictures, besides revealing cloud patterns which were obvious in the original picture, also revealed patterns which tended to be obscured by the more dominant features. Most significantly, the technique

has provided a means to quantitatively describe the "vermiculated" patterns and the differences which occur in them from time to time and place to place. The continuation of this study is aimed at using these spectral analyses along with conventional meteorological observations in an effort to find the significant physical parameters which contribute to the makeup of the entire cloud pattern.

ACKNOWLEDGEMENTS

The authors are especially grateful to the assistance of Mr. Barry Wolman, who programmed all the machine computations, and Mr. Allan H. Murphy, who performed the statisitical analysis of the Monte Carlo experiments. Some of the computations were carried out on the computer facilities of the National Center for Atmospheric Research, where one of the authors spent the summer of 1962 as a visitor; most of the machine computations were performed through the facilities of the Computing Center of the University of Michigan. The authors are appreciative of the availability of these facilities for their work.

PART II

THE NATURE OF PHYSICAL PARAMETERS AFFECTING CONVECTIVE TRANSFER PROCESSES

DATA

TIROS has served to bring the cumuliform cloud patterns in the range of 25 to 100 miles, to the attention of the meteorologist. The general synoptic conditions conducive to the formation of these patterns have been ascertained by Krueger and Fritz (1961). A means of extending the knowledge about these particular cloud patterns is by examining the quantitative differences (or lack thereof) which occur at different times and places, as determined by the spectral analysis techniques, and relating these differences to the physical parameters which are thought to be important in the formation of these clouds. One of the major difficulties to be expected with this type of approach is the paucity of conventional meteorological information available in certain areas. It is well known that ships tend to congregate in well marked "lanes" depending on their destination with not too many ships traveling outside these lanes.

The particular cloud patterns of interest to us are quite common over the oceans, as shown by the TIROS photographs. The pictures analyzed up to now have been those taken by TIROS I during the spring of 1960. These pictures contained the cloud patterns associated with the moving anticyclones of mid-latitudes. The lack of conventional meteorological data over most of the oceans outside of the normal shipping lanes preclude the selection of pictures to be analyzed based on picture content alone. Thus, the study of the cloud patterns associated with these moving anticyclones is restricted to those times

when they happen to be in the regions of the Atlantic and Pacific shipping lanes. It is anticipated that future studies will utilize the pictures available from TIROS III during the summer of 1961 as well as those of TIROS V during the same period in 1962. This will eliminate the restriction of studying only those "vermiculated" cloud patterns associated with these moving anticyclones. The conditions favorable for the formation of these cumuliform cloud patterns are found as almost "steady state" conditions in some parts of one of these shipping lanes in summer, e.g., the northeast trades of the Pacific Ocean between the United States and Hawaii. Surface observations of such physical parameters as wind speed and direction, and air-sea temperature differences should be sufficient in this area for this type of analysis. A limited number of upper air observations are also available over this region.

CELLULAR CONVECTION

Some of the most marked cellular cloud areas occur in association with the inversions produced by the sub-tropical high pressure areas of the Eastern Pacific and Atlantic oceans. In most of the cases examined, there is a heat flux from the ocean to the atmosphere with the convective activity capped by the inversion. This would suggest that the mechanism producing cellular convection is an efficient means for transferring energy stored in the oceans to the atmosphere in the region of the sub-tropical anticyclones.

In mid-latitudes, particularly in winter, when cool air moves over warmer water violent convective activity frequently occurs with the formation of towering cumulus at times. In this case there is rarely an inversion capping the convective activity or if there is one it is weak and easily broken down.

However, in the regions of the sub-tropical highs it is rare for such violent convective activity to occur and thus it would be reasonable to expect cellular convective activity capped by an inversion to be the dominant form of convective activity and hence the dominant energy transfer mechanism.

Experimental and theoretical investigations of cellular convection have been carried out since the first controlled laboratory investigations of H. Benard in 1900 and 1901. Most of the theoretical studies have been extensions of the classical work of Lord Rayleigh (1916). Of particular interest to asmospheric studies is the case when rotation of the liquid or gas is considered, this problem has been considered by Jeffrey's (1928) and in more detail by Chandrasekhar (1953). Nakagawa and Frenzen (1955) appear to be the first to have conducted detailed experiments for the case of rotating liquids and gases. The great difficulty in theoretical investigations is the non-linearity of the differential equations, hence various assumptions have to be made to linearize the equations so that some form of analytic solution may be obtained; this needless to say introduces considerable difficulty in interpreting the solutions.

Experimental work on cellular convection indicates that for Benard cells the diameter-depth ratio is of the order of 2 for shallow convection and about 0.5 for deeper convections; on the other hand the cellular patterns observed by TIROS I have diameter-depth ratios of the order 10 to 20. Undoubtedly Benard cells do occur in the atmosphere although they are probably obscured by wind shear and uneven heating effects, most of the time. On examining the larger cells observed by TIROS I there is a microstructure evident which may be related to Benard cells but the theory does not indicate why larger cells

should be formed. Nakagawa and Frenzen (1955) have considered an overstable mode as one solution to their equations and suggest that an interference between the normal and overstable modes may produce larger areas of cloud but even these are quite a bit smaller than the TIROS I observations.

HEAT FLUX AND CELLULAR CONVECTION

It seems reasonable to assume that the flux of heat from ocean to atmosphere would have some bearing on the cell distribution and size. A method is given in a later section for evaluating the heat flux from the ocean. The latent heat flux turns out to be an order of magnitude larger than the sensible heat flux for the conditions of interest.

It is instructive to carry out a dimensional analysis of the relationship between the total heat flux Q and the various elements which appear physically significant.

Thus we write,

$$Q = f\left(D, h, d, k, \mu, c_p, \Omega, \rho, \gamma, \frac{\partial \bar{v}}{\partial z}\right)$$

where

Q = latent heat flux

h = depth of cell

D = diameter of cell

T = Taylor number $= 4\Omega^2 h^4/\nu^2$

P = Prandtl number $= \nu/\kappa$

$\gamma = \frac{-\partial\theta}{\partial z}$ where θ is the temperature

c_p = specific heat at constant pressure for air

Ω = angular velocity

k = thermal conductivity for air

$\kappa = k/\rho\, c_p$

μ = viscosity of air

ν = μ/ρ

ρ = density of air

$\bar{v}$ = mean wind speed.

A standard dimensional analysis yields

$$\frac{4Q}{h\mu\Omega^2} = f(\tfrac{1}{2}\sqrt{T}\ ,\ \frac{D}{h}\ ,\ \frac{d}{h}\ ,\ P^{-1},\frac{\gamma c_p}{h}\ \Omega^2\ ,\ c_p\gamma/h(\frac{\partial\bar{v}}{\partial z})^2)\ . \qquad (19)$$

If we consider Ω as a rotation about the vertical, then $4\Omega^2 = 4(\Omega' \sin\phi)^2 = f^2$, where ϕ is the latitude, Ω' is the earth's rotation, and f is the Coriolis parameter. However, the atmosphere generally possesses a rotation of its own relative to the earth, hence a better approximation to $4\Omega^2$ is

$$(f + \zeta_r)^2 = \zeta_a^2$$

where ζ_r and ζ_a are the relative and absolute vertical components of the vorticity, respectively. Thus $\Omega = \tfrac{1}{2}\zeta_a$ and we can write (19) as

$$\frac{4Q}{h\mu\zeta_a^2} = f(\tfrac{1}{2}\sqrt{T}\ ,\ P^{-1}\ ,\ \frac{D}{h}\ ,\ \frac{d}{h}\ ,-\frac{c_p}{h}\frac{\partial\theta}{\partial z}\ (\frac{\zeta_a}{2})^2\ ,\ c_p\gamma/h(\frac{\partial\bar{v}}{\partial z})^2). \qquad (20)$$

The Taylor number T gives a measure of the effect of rotation. The Prandtl number P indicates the importance of viscosity and conductivity in the liquid or gas, for air $P = 0.77$ and, since it is constant, it need not be considered further in this investigation, although Nakagawa and Frenzen (1955) have discussed the significance of this parameter for the various types of convectional instability which may arise in a rotating fluid. The term $-\frac{c_p}{h}\frac{\partial\theta}{\partial z}(\frac{\zeta_a}{2})^2$ is rather difficult to interpret. For an adiabatic lapse rate $\frac{\partial\theta}{\partial z} = -\frac{g}{c_p}$ so the term becomes $\frac{g}{h}(\frac{\zeta_a}{2})^2$. In the lower levels of the troposphere, if there is convective activity then the lapse

rate would be adiabatic or slightly greater and thus this term gives a relation between the cell depth and the absolute vorticity.

The term $c_p \frac{\gamma}{h} (\frac{\partial \bar{v}}{\partial z})^2$ is a form of Richardson's number. It indicates that wind shear might be an important parameter for this problem.

The Rayleigh number, defined by

$$R = \frac{\alpha \gamma g h^4}{\kappa \nu}$$

where α is the coefficient of thermal expansion, enters into most of the theoretical discussions in connection with the onset of instability. Nakagawa and Frenzen (1955) consider a critical Rayleigh number in connection with overstable oscillations. The Rayleigh number does not appear to be very significant in the problem under consideration, but it could easily be taken into account.

With the aid of the results yielded by the spectrum analysis (Part I) it will be possible to examine the relationships envisaged in equation (20) using statistical techniques such as multiple regression. Knowledge of the relevant physical parameters should make further physical-dynamical investigations more profitable.

DETERMINATION OF SENSIBLE AND LATENT HEAT FLUXES

Theoretical Considerations

Sverdrup (1957) gives a discussion of the flux of water vapour and sensible heat from the sea surface. It is assumed that the flux of water vapour is independent of height z in the region 10 to 20 meters above the sea surface. The flux F is then given by

$$F = \rho K \frac{dq}{dz} = \text{constant} \tag{21}$$

where ρ is the density of the air, q is the specific humidity and K is the eddy diffusivity in the air. If the flux is upward then there is evaporation and

$$E = -\rho K \frac{dq}{dz} \tag{22}$$

where E is the evaporation.

Theoretical and laboratory studies indicate that

$$K \sim k_o \gamma_z v_z z \tag{23}$$

where $k_o = 0.4$ (von Karman's constant), γ_z^2 is the roughness coefficient (defined by G.I. Taylor as $\tau = \gamma_z^2 \rho v_z^2$, where τ is the stress and v_z is the velocity at height z). The subscripts z and zero refer to values at height z above the surface and at the surface respectively.

R.B. Montgomery (1940) examined evaporation from sea surfaces and specified the humidity in terms of an evaporation coefficient, viz:

$$\Gamma_z = - \frac{1}{q_o - q_z} \frac{dq}{d(\ln z)} \quad . \tag{24}$$

Using the above relations, equation (22) can be written as:

$$E = \rho k_o \gamma_z v_z (q_o - q_z) \Gamma_z \quad . \tag{25}$$

The choosing of a value for Γ_z poses some difficulty. This problem has been discussed in some detail by Sverdrup (1951). He favors the assumption that next to the sea surface there exists a thin layer, the thickness of which is inversely proportional to the wind velocity, through which water vapor is transported upwards by molecular diffusion. Above this layer eddy diffusion transports the water vapor. This argument seems

reasonable for a fairly smooth surface; since the sea is rarely smooth the above argument would run into some difficulty. Sverdrup argues that essentially the same process takes place even when the sea surface is rough. If a small air parcel hits the surface it may lose all its momentum but it will not immediately reach the specific humidity of the surface. If it remains at relative rest in one of the depressions of the rough surface its water vapor content will increase due to molecular diffusion. This means that essentially a process similar to that prevailing over a smooth sea surface will prevail provided that a statistical diffusion layer is considered to exist.

Montgomery (1940) makes different assumptions. His final results for the evaporation are low in comparison to rather crude observations that have been carried out, while Sverdrup's theory gives results closer to the observed values for evaporation.

The flux of the latent heat is given by

$$Q_e = LE \tag{26}$$

where L is the latent heat of vaporization (=585 cal/gm). Using Sverdrup's theory we obtain

$$Q_e = (q_o - q_z)\, v_z \times 10^{-3} \text{ cals/sq. cm/sec} \tag{27}$$

where v_z is measured in cm/sec and q_o, q_z in gm/gm. By reasoning similar to the above the flux of sensible heat can be written

$$Q_s = (c_p \rho k_o \gamma_z v_z)(T_o - T_z) \tag{28}$$

where T_o and T_z are the temperatures at the surface and at the height z. Substituting values into this equation gives

$$Q_s = 4.16 \times 10^{-7} (T_o - T_z) \cdot v_z \quad . \qquad (29)$$

(cf. Riehl et al. (1951)

On substituting appropriate values into equation (29) the results are at least an order of magnitude smaller than Q_e and could be neglected since the computations of Q_e are not all that accurate.

Practical Determination of Q_e and ζ_a

To obtain values for Q_e it is of course necessary to rely on the synoptic reports of various ships. These reports will have varying degrees of accuracy and it seemed reasonable to assume that a graphical method would be the best for obtaining isopleths of Q_e since the smoothing inherent in such methods is desirable. It was assumed that measurements of temperature and dewpoint on the ships' decks were representative of the values pertaining in the turbulent layer. Also it was assumed that the air was saturated in a thin layer in contact with the sea surface, i.e., q_o would be the saturated value for the prevailing water temperature and atmospheric pressure.

The technical details for preparing the isopleths of Q_e are as follows:

1. Isopleths of water temperature are drawn using ships synoptic reports, reports covering one day or even longer can be used since there is very little change in water temperature from day to day.
2. Isopleths of q_o (specific humidity at the sea surface) can be prepared from chart 1 assuming that saturated conditions prevail at the sea surface. The Smithsonian Meteorological Tables were used to obtain the q_o's and q_z's (List, 1958).

3. Isopleths of dew point using ships' observations were prepared (for a particular synoptic hour).
4. Isopleths of q_z (specific humidity at the ship's deck) were prepared using chart 3.
5. Chart 4 is graphically subtracted from chart 2 to give $(q_o - q_z)$.
6. An isotach analysis (in meters/sec) is obtained from the surface chart. The isotach analysis required some care since numerous reported winds did not agree too well with the gradients; however some decision as to a reasonable value could be generally reached.
7. The charts 5 and 6 could be graphically combined to produce

$$Q_e = (q_o - q_z) \cdot v_z \times 10^{-3} \text{ (in cals/sq. cm/sec)} .$$

The graphical techniques developed by Fjortoft were used to determine the absolute vorticity at the 1000 mb level. Essentially, this involves a graphical solution to the equation

$$\zeta_a = \frac{-4gm^2}{fH^2} (z - \bar{z}) + f \qquad (30)$$

where m is the scale factor of the chart used, H is the smoothing interval, z is the height field of the 1000 mb. surface, $\bar{z}$ is the space-mean of this 1000 mb. surface, and f is the Coriolos parameter. The first term on the right-hand side is an expression for the geostrophic relative vorticity ζ_r. The mechanical procedure used in obtaining graphical solutions to this equation is described in detail by Petterssen (1956). In determining the solution to equation (30), it was assumed that the scale factor of the chart used was constant at a value of 1.1 over the intervals of latitude used. A smoothing interval of 800 km was used for the value of H.

The methods outlined above were used in evaluating the latent heat flux from the water to the air and the absolute vorticity at 1000 mb on days when there appeared to be cellular convection present. Two cases are shown as examples of the values obtained by this method. The first illustrates a case associated with a moving anticyclone in the Western Atlantic during April 1960. This case has been investigated by Krueger and Fritz (1961) who also give isopleths of the height of the subsidence inversion. The second case shows an example of the values of the latent heat flux and absolute vorticity obtained in the region of the Northeast trades of the Pacific Ocean during May 1960.

The synoptic situation prevailing during the Atlantic case is illustrated by the Surface Analysis for 1200Z April 4, 1960 shown in Figure 21. This is approximately the middle of the period used in the analysis of the physical parameters associated with this moving anticyclone. Figures 22, 23 and 24 give values of the difference between the water and air temperatures existing on three separate days. The isopleths of latent heat flux for two times during the period are shown in Figures 25 and 26. A comparison of the values for the difference between the water and air temperatures and the latent heat flux shows that maximum latent heat flux does not necessarily correspond to maximum water-air temperature differences and why it is important to consider the latent heat flux rather than water-air temperature differences when considering the cellular cloud formations.

The 1000 mb charts used in determining the vorticity at this level are drawn by interpolation from the surface analysis taking 3.75 mb to correspond to 100 ft. Figure 27 shows the 1000 mb chart obtained by this method for 0000Z May 22, 1960. The

values obtained for the absolute vorticity at this level and time, as determined by Fjortoft's graphical techniques, are shown in Figure 28. The absolute vorticity for the 1000 mb level at the same time and covering the same area as the surface analysis (Figure 21) is shown in Figure 29.

The water-air temperature differences and the latent heat flux values prevailing over the Eastern Pacific area are shown in Figures 30 and 31. The areas of cellular convection as determined from TIROS I photographs for the Atlantic and Pacific cases are delineated by the dashed curves in Figures 25 and 31, respectively. The evidence of these figures tends to confirm the expectation that the areas of cellular clouds are associated with regions of maximum heat flux. The aim of future investigations will be to determine if any relationship exists between cell sizes and heat flux and also if there is a relation between the vorticity and the cell sizes.

CONCLUSION

The nature of convective transfer processes in the atmosphere and the interaction of the oceans and the atmosphere are subjects in which meteorologists freely admit to a lack of knowledge. The advent of the meteorological satellite has presented visible evidence of these processes at work. The realization of the potential value of satellite pictures of these cloud patterns awaits the meteorologist's ability to interpret them in terms of the physical parameters causing their formation.

Parameters which appear to be physically significant in cellular convection are large in number and easy to designate. Theoretical and laboratory investigations have served as an aid in pointing out the relative importance of these parameters in the atmosphere. The relationship between these parameters and

and their contribution to the determination of the cloud patterns and sizes as shown by the TIROS photographs can only be ascertained by looking at large numbers of cases and applying careful physical reasoning and statistical analysis.

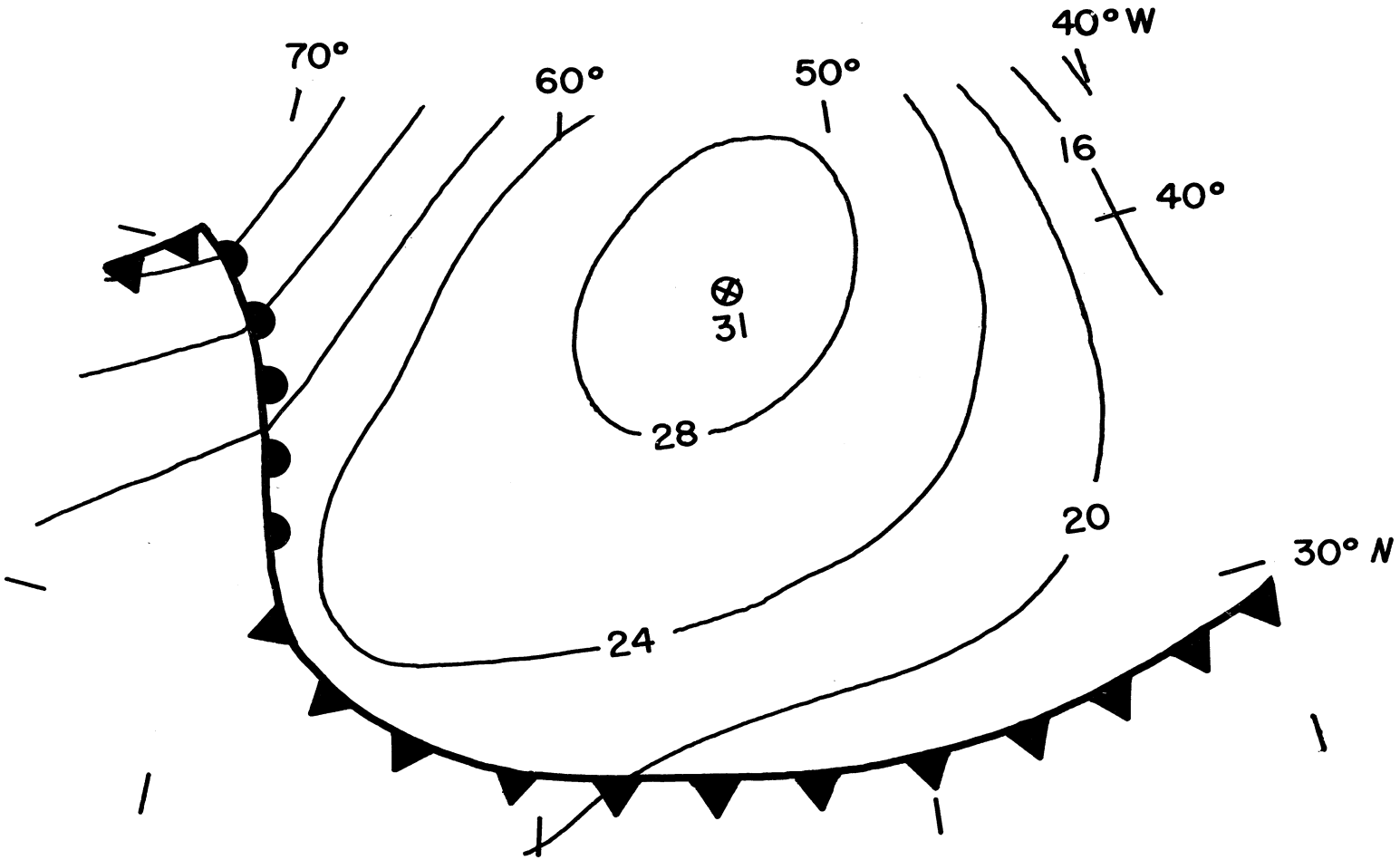

Figure 21. Surface analysis 1200Z, April 4, 1960.

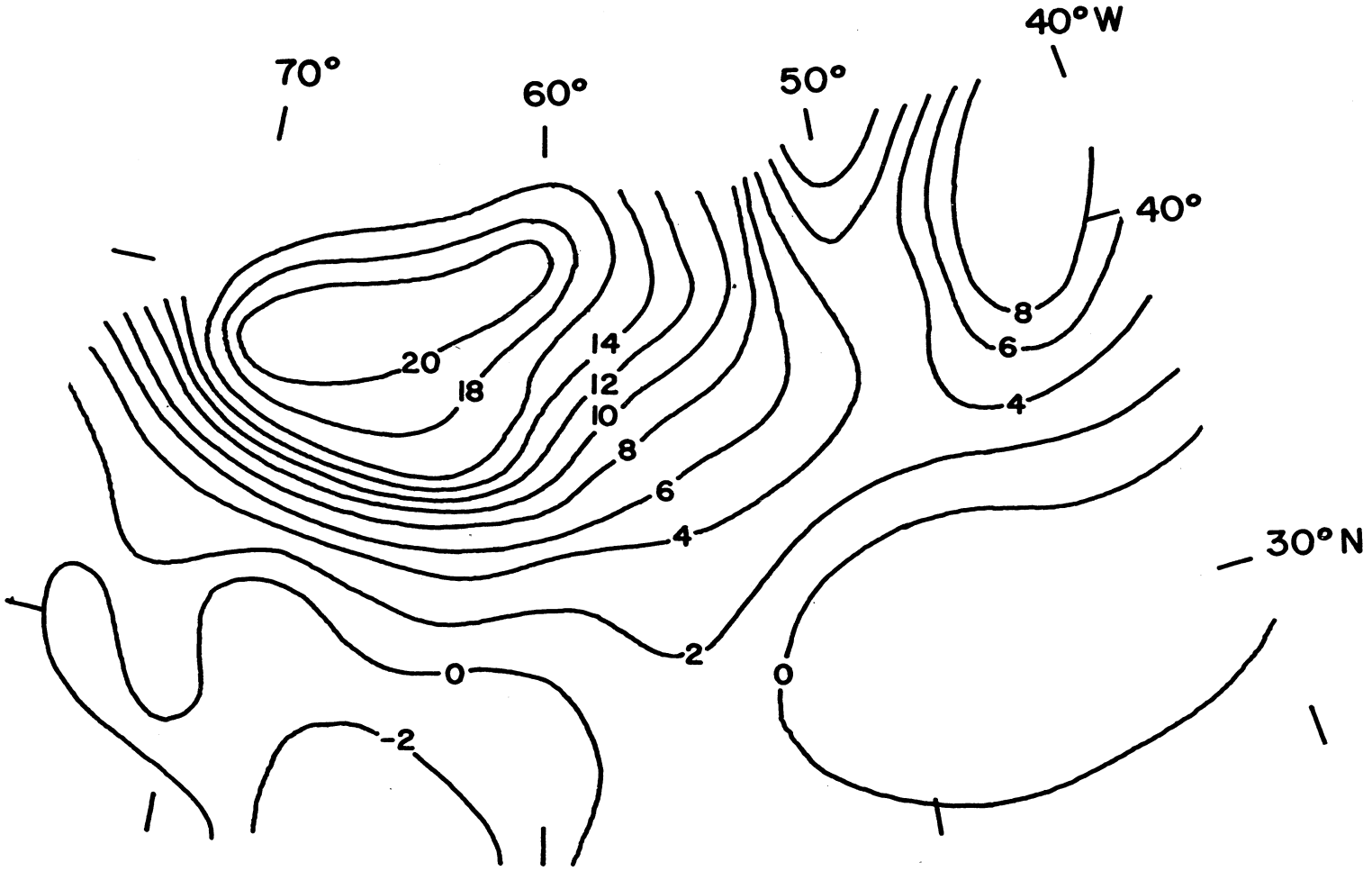

Figure 22. Water temperature minus air temperature (°F) 1200Z, April 3, 1960.

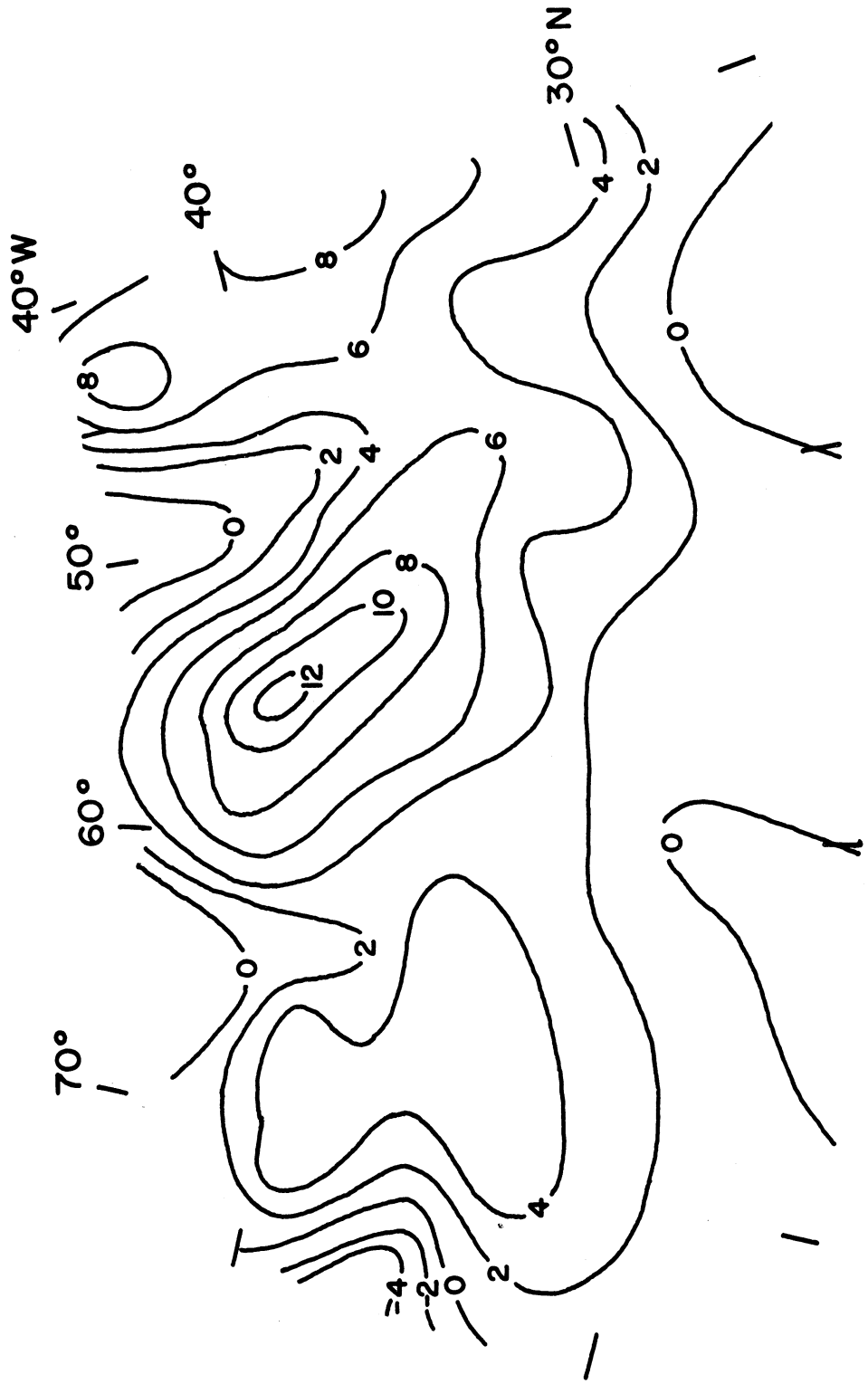

Figure 23. Same as Figure 22 for 1200Z, April 4, 1960.

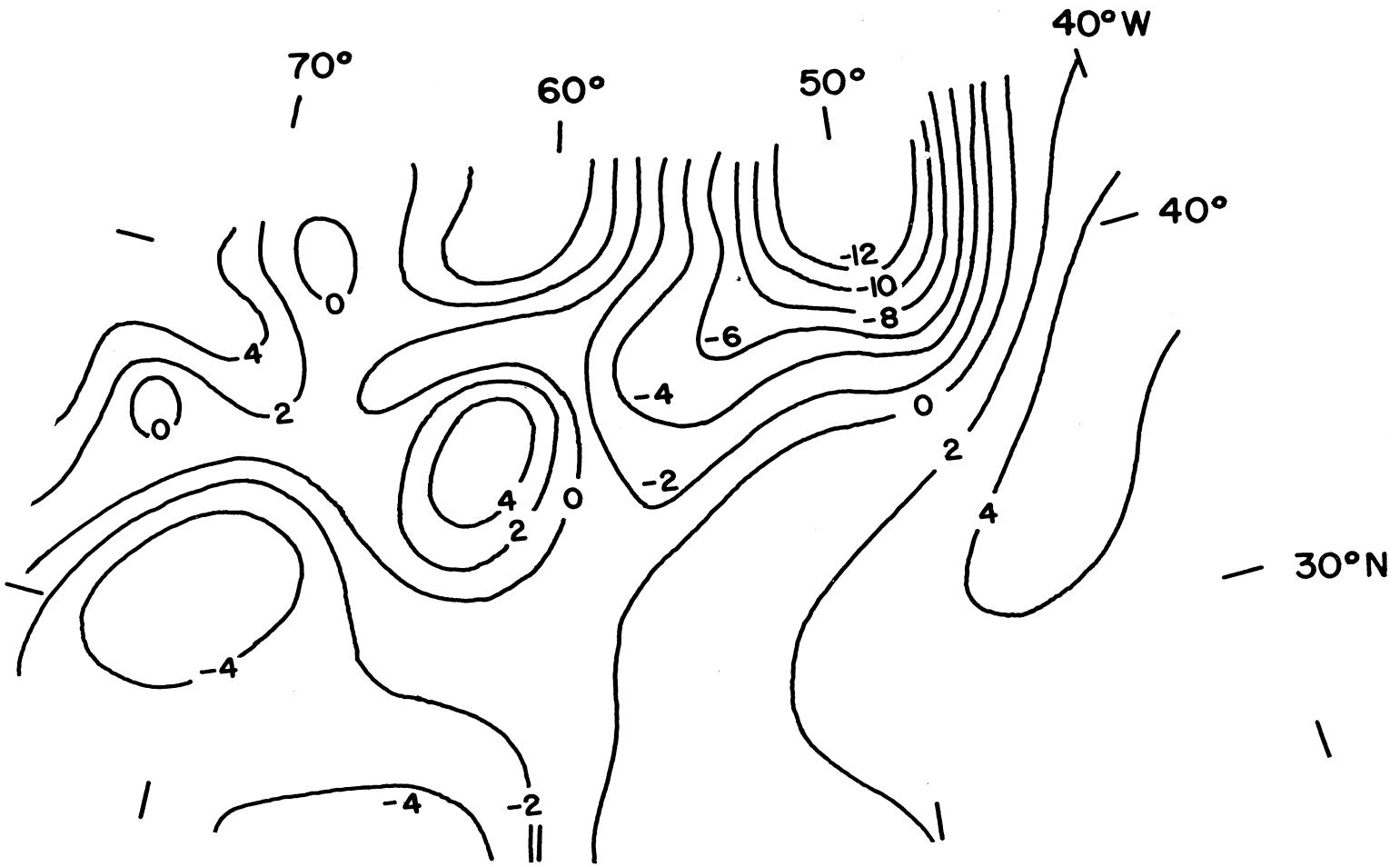

Figure 24. Same as Figure 22 for 1200Z, April 5, 1960.

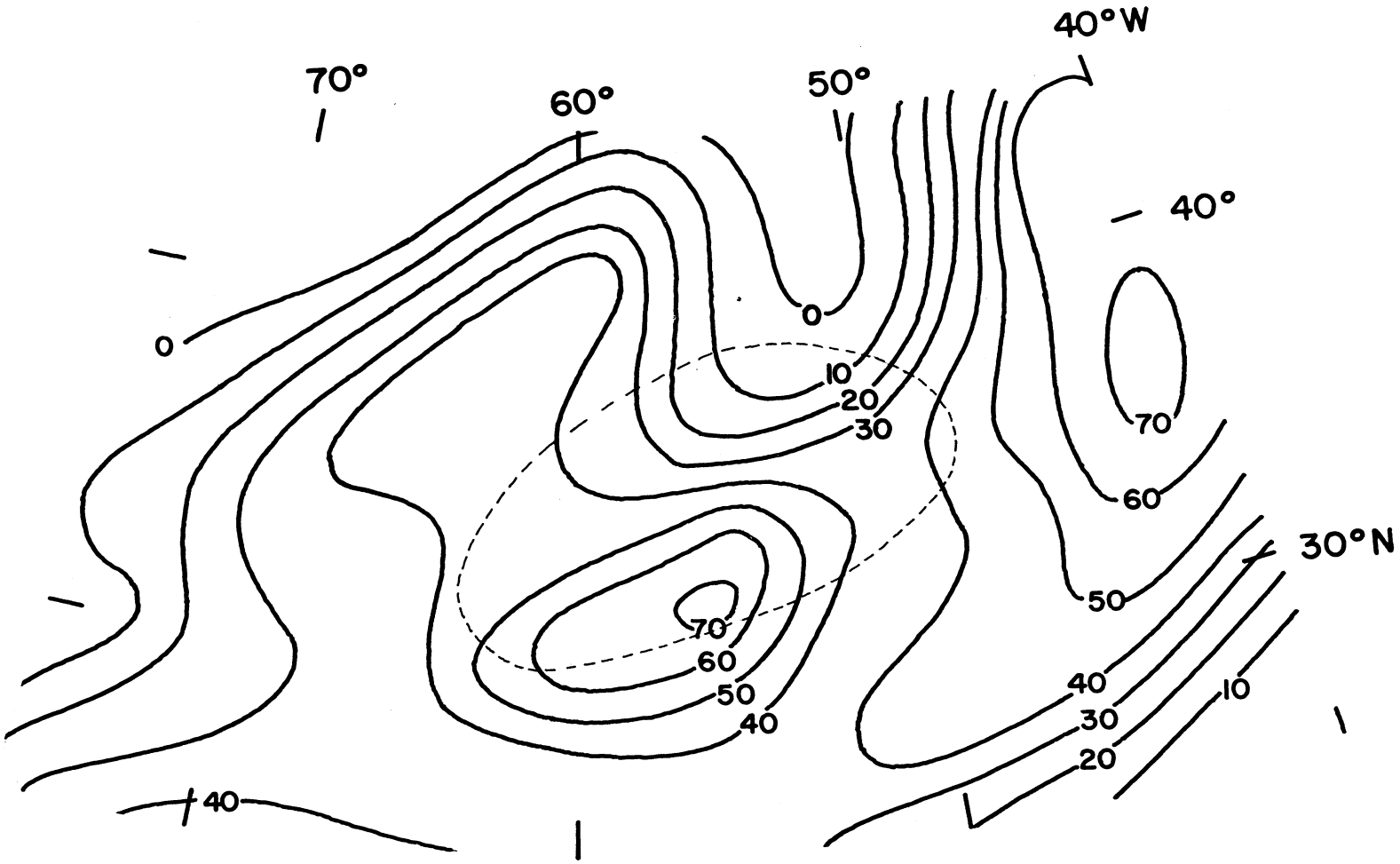

Figure 25. Latent Heat Flux in cals. cm^{-2} sec^{-1} × 10^{-5} for 1800Z, April 4, 1960. (-------area of Cellular Convection).

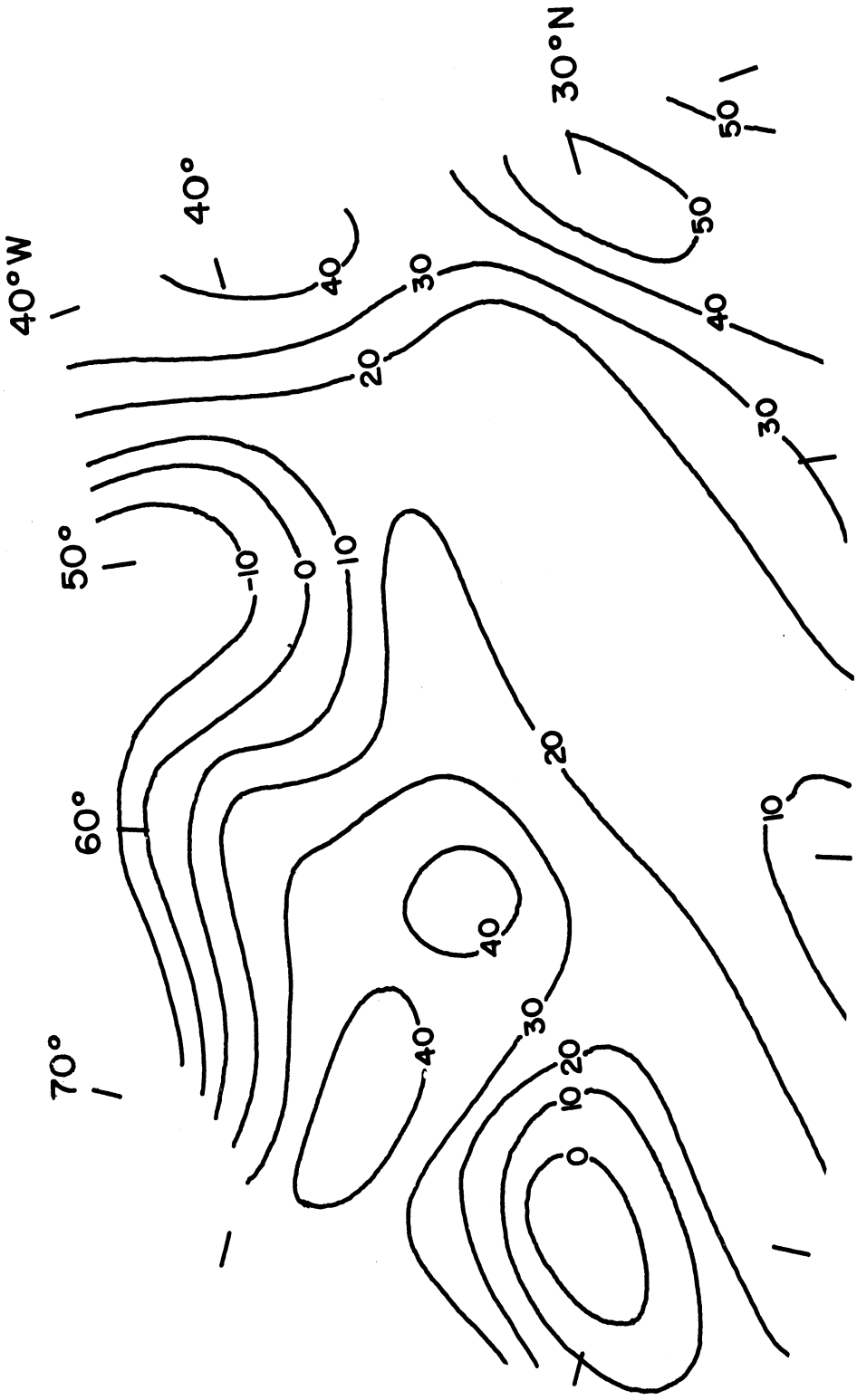

Figure 26. Same as Figure 25 for 1200Z, April 5, 1960.

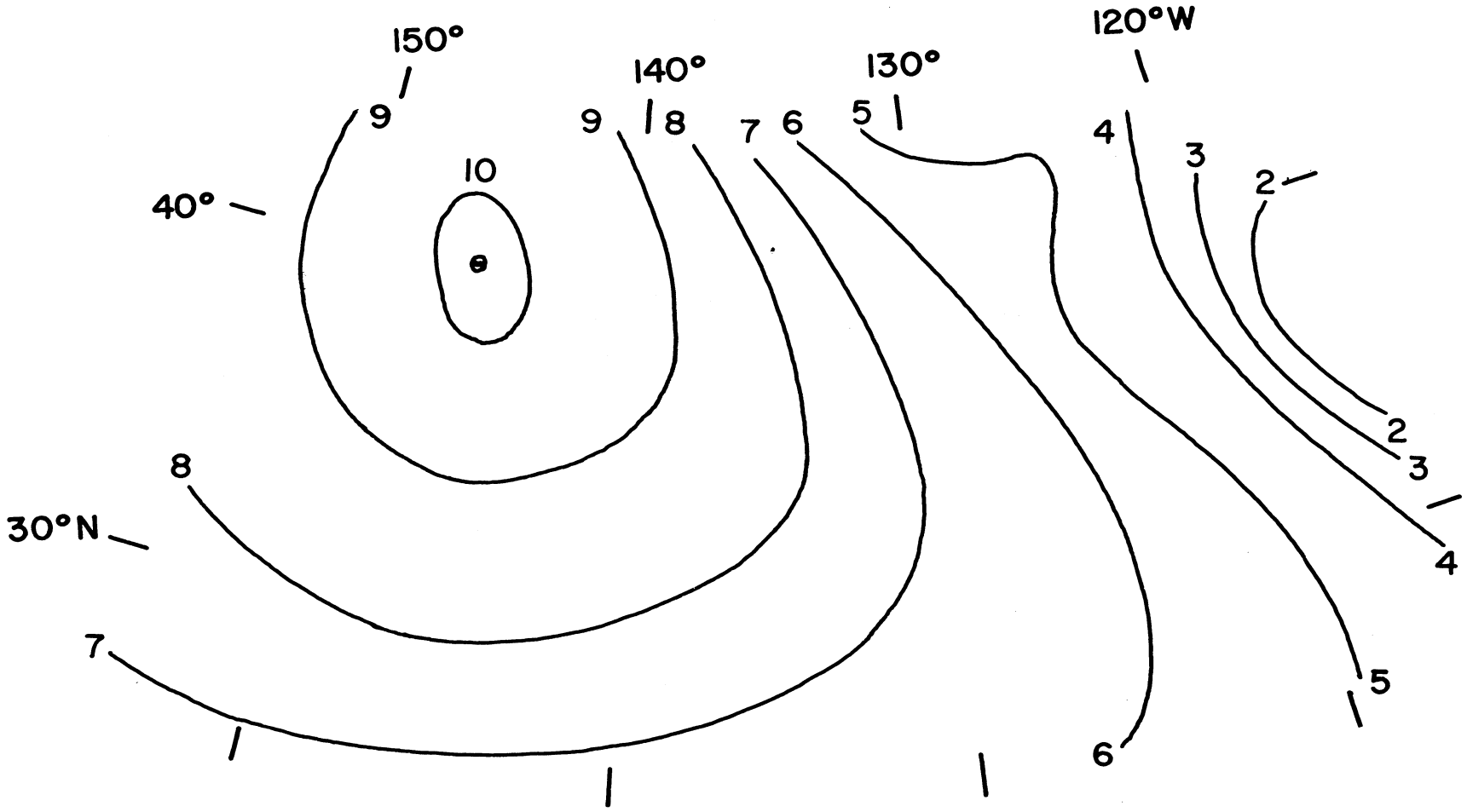

Figure 27. 1000 mb analysis (× 10^2 ft) 0000Z, May 22, 1960.

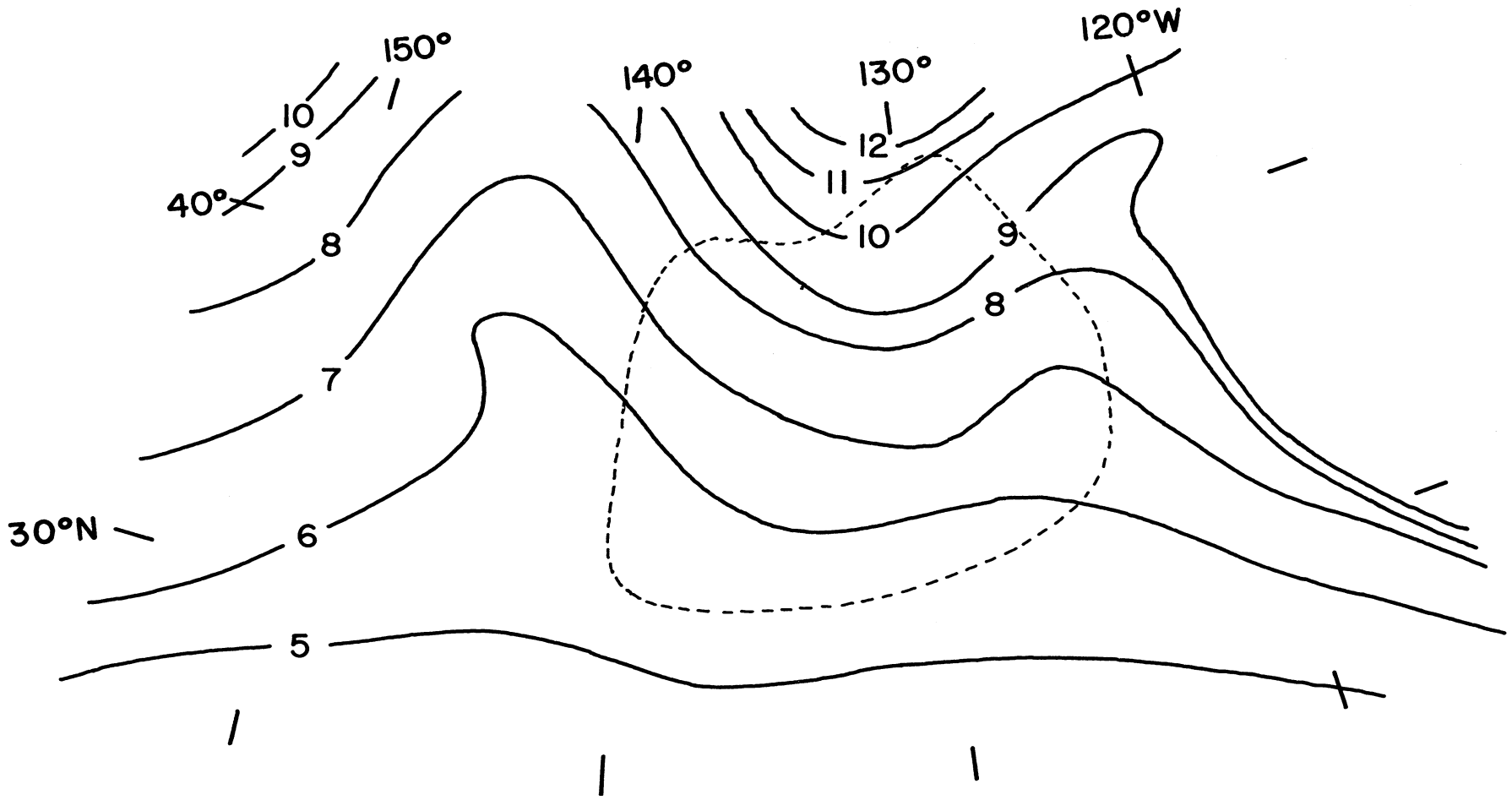

Figure 28. Absolute Vorticity (ζ_a) at 1000 mb (10^{-5} sec^{-1}) 0000Z, May 22, 1960.

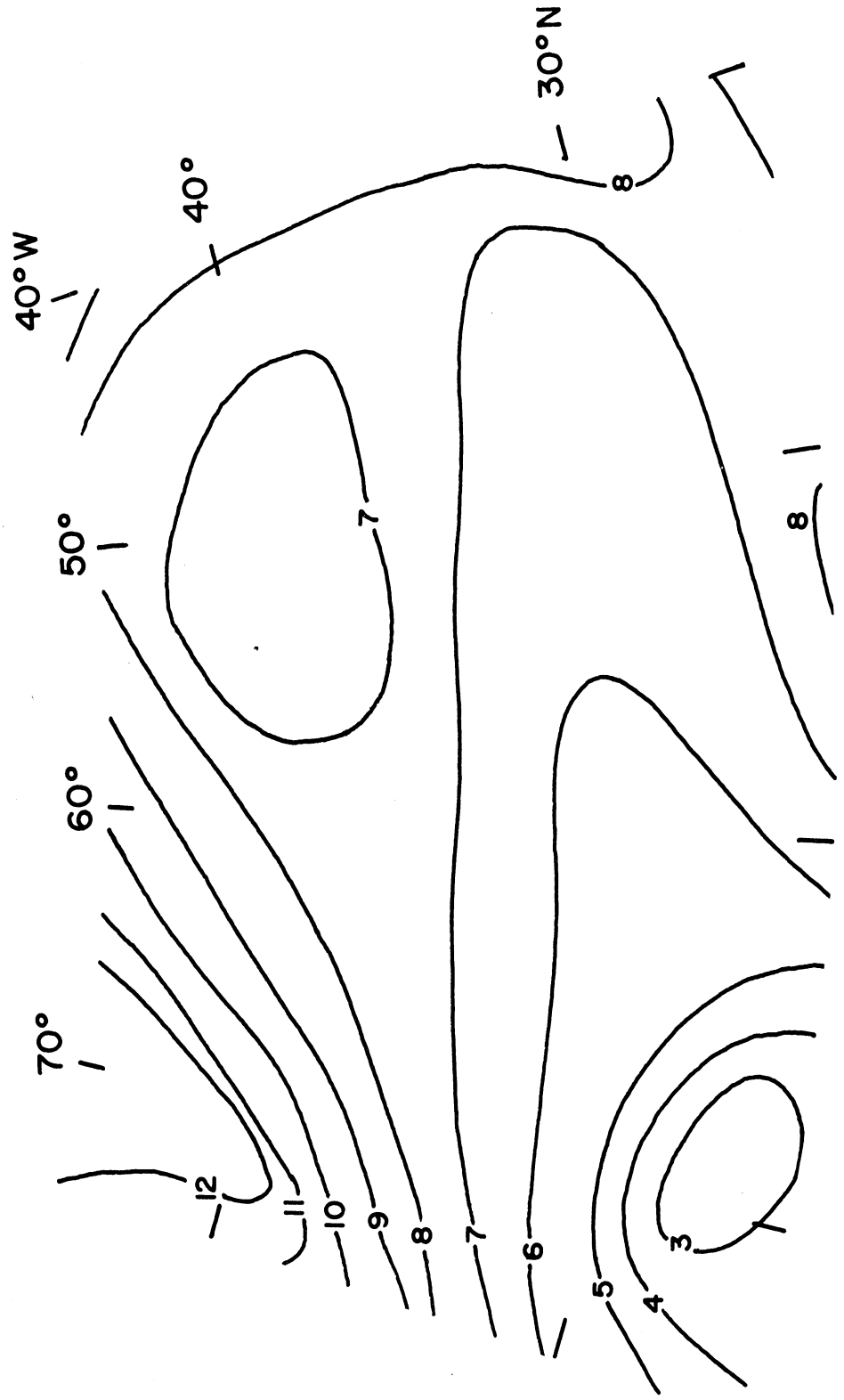

Figure 29. Same as Figure 28 for 1200Z, April 4, 1960.

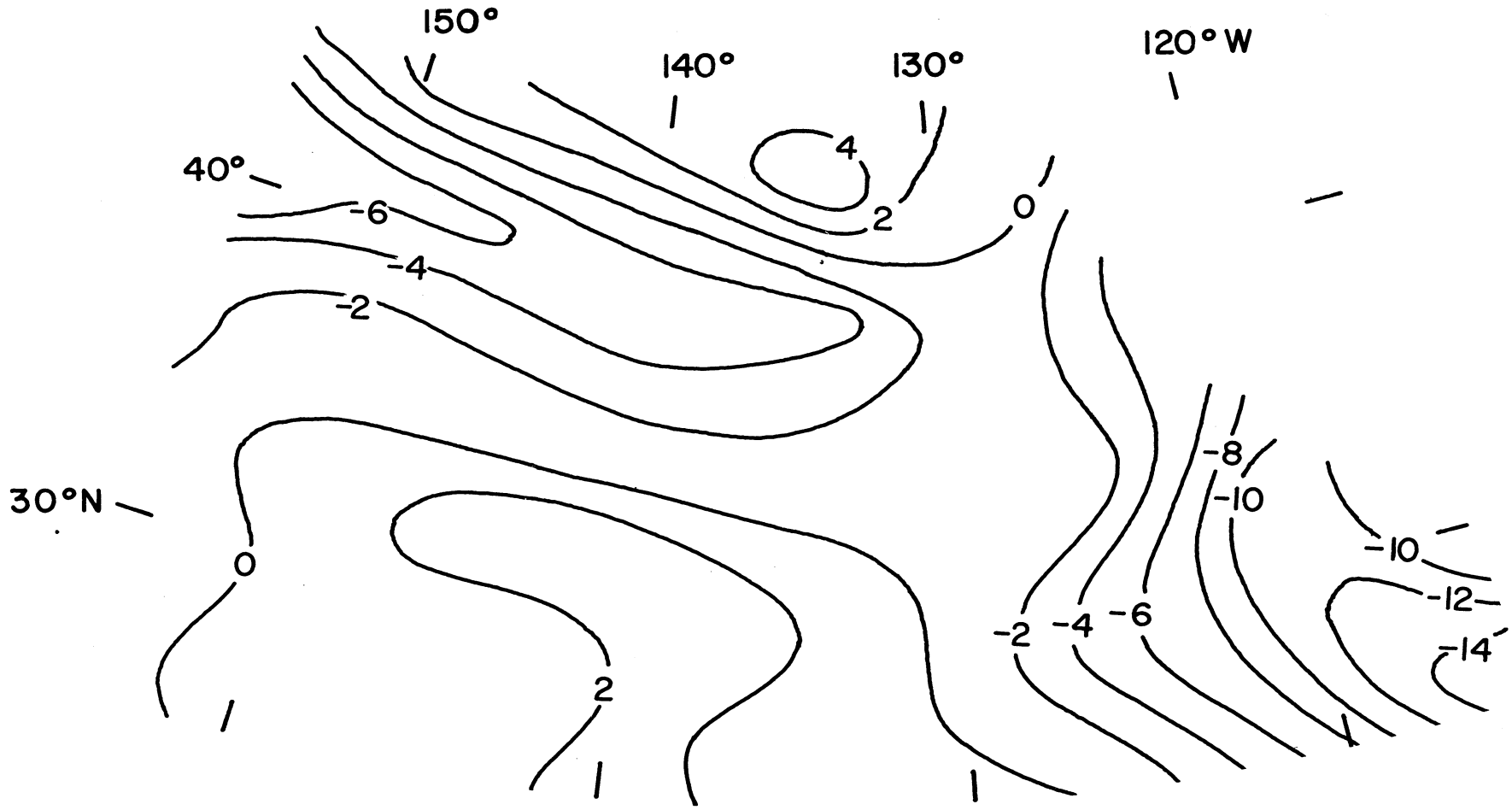

Figure 30. Same as Figure 22 for 0000Z, May 21, 1960.

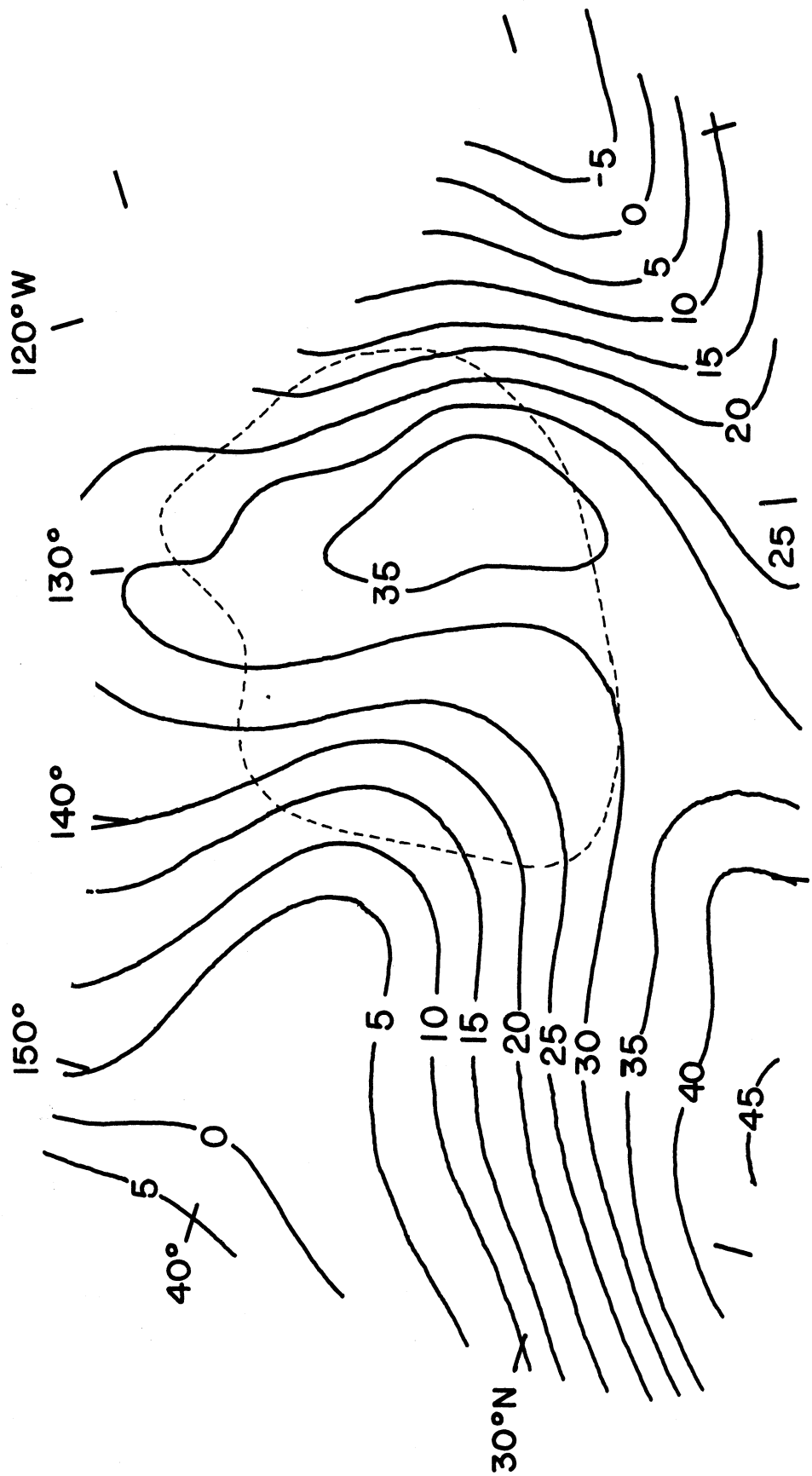

Figure 31. Same as Figure 25 for 0600Z, May 21, 1960.

REFERENCES

Blackman, R.B., and Tukey, J.W., 1958: The Measurement of Power Spectra. Dover Publications, Inc., New York, 180 pp.

Chandrasekhar, S., 1953: The instability of a layer of fluid heated below and subject to Coriolis forces. Proc. Roy. Soc. (A), 217, 306-327.

Conover, J., 1962: Cloud Interpretation from Satellite Altitudes. GRD Research Note No. 81, AFCRL-62-68, 77 pp.

Cote, L.J., et al, 1960: The Directional Spectrum of a Wind Generated Sea as Determined from Data Obtained by the Stereo Wave Observation Project, edited by W.F. Pierson, Jr., Meteorological Papers, Vol. 2, No. 6, 88 pp., New York

Griffiths, H.L., Panofsky, H.A., and Van der Hoven, I., 1956: Power Spectrum Analysis Over Large Ranges of Frequency. Journal of Meteorology, 13, pp. 279-282.

Jeffreys, H., 1928: Some cases of instability in fluid motion. Proc. Roy. Soc. (A), 118, 195-208.

Krueger, A.F., and Fritz, S., 1961: Cellular Cloud Patterns Revealed by TIROS I. Tellus, 13, pp. 1-7.

Leese, J.A., 1962: The Role of Advection in the Formation of Vortex Cloud Patterns. GRD Research Note No. 78, AFCRL-62-286, 27 pp.

List, R.J., 1958: Smithsonian Meteorological Tables. Sixth Revised Edition, 527 pp.

Montgomery, R.B., 1940: Observations of vertical humidity distributions above the ocean surface and their relation to evaporation, Papers in Physical Oceanography and Meteorology, M.I.T. 7, no. 4.

Nakagawa, Y. and Frenzen, P., 1955: A theoretical and experimental study of cellular convection in rotating fluids. Tellus 7, 1-22.

Petterssen, S., 1956: Weather Analysis and Forecasting Volume 1 Motion and Motion Systems, 2nd edition McGraw-Hill Book Co., New York, 428 pp.

Rayleigh, Lord., 1916: On convection currents in a horizontal layer of fluid. Phil. Mag. 32, 529-546.

Riehl, H., et al. 1951: The North-east Trade of the Pacific Ocean. Quart. Journ. Roy. Met. Soc. 77, 598-626.

Sadler, J., 1962: Utilization of Meteorological Satellite Cloud Data in Tropical Meteorology. GRD Research Note. AFCRL-62-829; 40 pp.

Staff members, NASA and U.S. Weather Bureau, 1962: Final Report on the TIROS I Meteorological Satellite System. NASA Tech. Rep. R-131, 355 pp.

Sverdrup, H.U., 1951: Evaporation from the Oceans. Compendium of Met. Am. Met. Soc. 1071-1081.

Sverdrup, H.U., 1957: Oceanography. Handbuch der Physik, Vol. 48, Springer-Verlag, Berlin.

Timchalk, A., and Hubert, L.F., 1961: Satellite Pictures and Meteorological Analyses of a Developing Low in the Central United States. Monthly Weather Review, 89, pp. 429-445.

APPENDIX

Cloud Analysis Program

Definition of Terms

A	Array of spectral estimates resulting from the addition of cosine and sine terms. ($S(\mu,\nu)$ in text).
AVG	Controls inclusion of results for averaging.
B	Array of spectral estimates as a result of subtracting sine from cosine terms. ($S(\mu,-\nu)$ in text).
BC	Autocovariance array.
COMB	MAD subroutine used to compute the A and B arrays.
COUNT	Controls counting of values in cloud pattern.
COVAR	UMAP subroutine for computing the autocovariance coefficients.
END	Controls printing of averages.
GRAPH	MAD subroutine for printing spectral estimates along coordinates suitable for contour analysis.
LINES	Number of columns used on the pattern input cards when reading with the standard format.
MEAN	Mean of random normal pattern generated by computer.
MX	Maximum lag in the X-direction.
MY	Maximum lag in the Y-direction.
NOFLIN	Number of lines in cloud pattern.
NONLIN	Number of points per line in cloud pattern.
NUMX	Factor by which input pattern is to be reduced in the X-direction.
NUMY	Same as NUMX, for y-direction.
OMIT	Control for skipping parts of computer program when not needed.
P	Smoothed cosine power spectrum coefficient.

Q — Smoothed sine power spectrum coefficient.

RECTFY — MAD subroutine for smoothing when the pattern has been reduced.

S — Unsmoothed cosine power spectrum coefficient.

SMOOTH — UMAP subroutine for smoothing power spectrum coefficients.

SPEC — UMAP subroutine to compute the power spectrum coefficients.

STDEV — Standard deviation of random normal pattern generated by computer.

SUMBC, SUMP, SUMPSQ, SUMQ, SUMQSQ — Sums and squares of sums used in computing average results.

T — Unsmoothed sine power spectrum coefficient.

TYPE — Control for specifying the pre-processing function(s) to be used.

Details of the Computer Program

In an effort to streamline the computer program for the spectral analysis of cloud patterns, two languages available at the University of Michigan were combined. These were the Michigan Algorithm Decoder (MAD) and the University of Michigan Assembly Program (UMAP). Along with the development of the techniques for the spectral analysis of cloud patterns, a computer program has evolved which is capable of handling the actual cloud patterns, idealized cloud patterns (with or without noise), or even to generate its own data in the form of a random pattern. While the input required and the output produced can become quite involved, the computer program itself can be divided into two main parts; a PRE-PROCESS in which

numerous options are available to perform different operations on the data prior to entry into COMMON in which the spectral pattern is computed. We would be pleased to make available, upon request, complete binary decks for the IBM 7090, although we must point out that the input-output operations and certain calling sequences are based on the University of Michigan system.

PRE-PROCESS

A flow diagram for this part of the program is shown in Figure 32. The title card, which is mandatory, contains the title specified by the user. Any legal character may be punched, or the card may be left blank. The control card(s), also mandatory, is used to provide the values of the mandatory variables TYPE, MX, MY, NONLIN, NOFLIN, and LINES; the optional variables NUMX, NUMY, MEAN and STDEV; and the switches AVG, END, OMIT and COUNT. The data cards, when required, are in the form of single digits between 0 and 7 punched consecutively in columns 1-N, where (N<73) is specified by LINES.

Provision has been made for the user specifying a special format which will apply to only one data set. This is done by making the value of LINES negative, and placing a single format card immediately preceding the data cards. Such a format would be used, e.g. in the case where an increase in the data interval is accomplished by reading only certain values and skipping M data points between the values used in the X and/or Y directions. This would effectively increase the data interval by $(M+1)\Delta x$ and/or $(M+1)\Delta y$.

The pre-processing operations actually performed depends on the value(s) of the variable TYPE. Any one, or any combination, of the pre-processing functions listed below may be used.

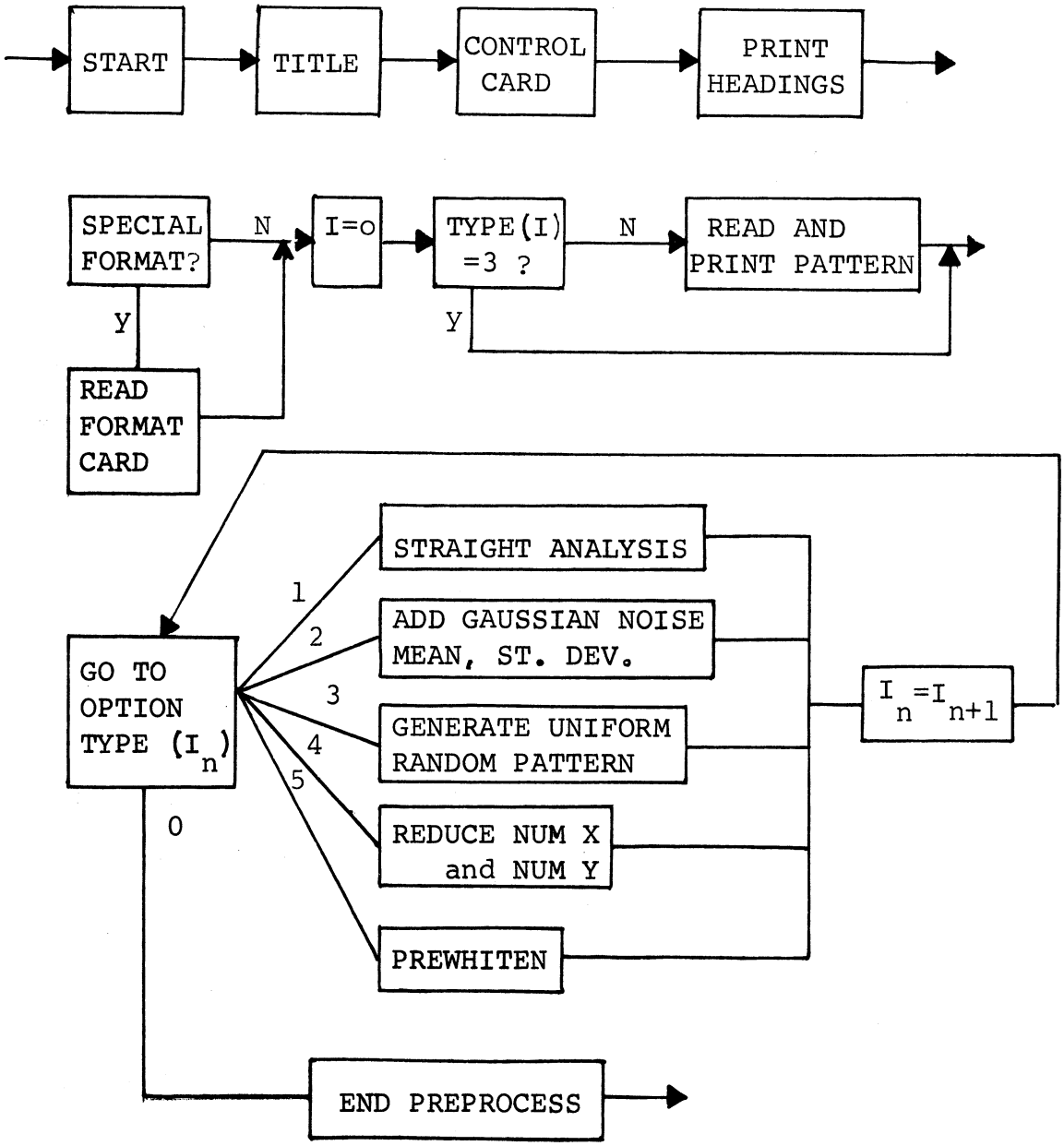

Figure 32. Flow diagram for PRE-PROCESS part of computer program.

1. No pre-processing is performed. Spectral analysis computed for pattern as given by data cards.
2. A noise in the form of a normally distributed set of random numbers is added to the input pattern. The resulting element will be an integer between 0 and 7. The MEAN and STDEV of the random pattern is specified by the user. This option was also used to generate the Gaussian distributions used in the Monte Carlo experiments.
3. The pattern is generated by the computer. Each element of the pattern will be an integer between 0 and 7 from a uniformly distributed random set. Since the reading of the internal clock and several other registers are sampled before the sequence is generated, different patterns will be generated on successive runs of the program. This option provided the uniform distributions used in the Monte Carlo experiments.
4. The input pattern is reduced through non-overlapping averaging, by the factor NUMX in the x-direction and NUMY in the y-direction. The reduction can be considered as a transformation which maps a block of NUMX - NUMY points into a single point. Effectively, this is an averaging technique so that the data interval is increased to NUMX (Δx) and/or NUMY (Δy). When this operation is called, a switch is set which later calls the subroutine RECTFY (see below).
5. The input pattern is "pre-whitened" by replacing each element by its deviation from the plane of best fit, where least square methods are used to fit the plane A + BX + CY to the data.

Up to 20 combinations of these five pre-processing functions can be specified at once. If it is desired to read the pattern, reduce it by the factor NUMX and/or NUMY, and pre-whiten the reduced pattern; the specifications would be TYPE = 4,5,0. The 0 indicates that the pre-processing is to be terminated and the data are in the final form for analysis.

COMMON

The program advances into the part termed COMMON only after encountering the variable TYPE = 0. The flow diagram for this part is shown in Figure 33 .

The variable COUNT comprises a conditional statement so that whenever its value is other than zero, the number of occurrences for each value of the integers 0 through 7 in the pattern are counted and printed. Any other values are treated as if they were equal to 8. Although the final pattern is printed out, this variable provides a convenient final check on the pattern analyzed. It also serves as a cursory check for the subroutine generating the random numbers. Finally, it serves to give an approximation to the amount of cloud cover in the patterns used.

The autocovariance array, BC, is computed by a call to the UMAP subroutine COVAR and then printed. Whenever the value of the variable AVG is other than zero, the BC array just computed is added to the partial sum array SUMBC and saved for later averaging.

The UMAP subroutine SPEC computes the power spectrum arrays for the cosine (S) and sine (T). The S and T arrays are then smoothed by a call to the UMAP subroutine SMOOTH to

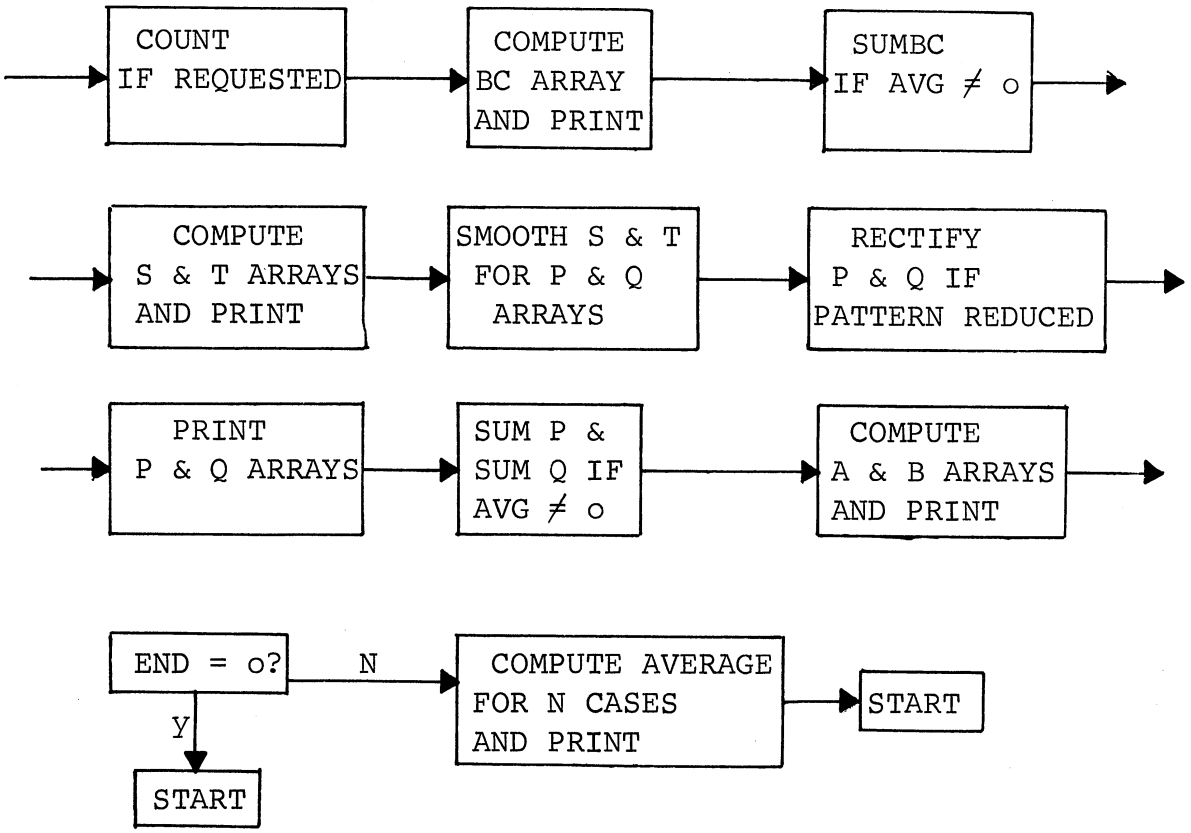

Figure 33. Flow diagram for COMMON part of computer program.

form the P and Q arrays. If the input pattern was reduced to form an average, the P and Q arrays are again smoothed by the subroutine RECTFY to take this into account. If the value of AVG is other than zero, the P and Q arrays and their squares are added to the appropriate partial sum arrays and saved for later averaging.

The spectral estimates, called A and B in the program, are the result of the addition and subtraction of the P and Q arrays. The UMAP subroutine GRAPH then combines the two arrays so that the final printout is arranged along coordinates suitable for contour analysis of the spectral estimates directly on the printout.

The partial sums of the arrays are saved so long as the value of AVG is other than zero, and the value of END is equal to zero. Whenever END is given a value other than zero, the mean for all the data sets included by the variable AVG is computed and printed.